International Journal of Biological Macromolecules 371 (2026) 152990

Contents lists available at ScienceDirect

International Journal of Biological Macromolecules

journal homepage: www.elsevier.com/locate/ijbiomac

Diepoxyoctane-cross-linked and spermidine-functionalized chitosan beads for the removal of hexavalent chromium and reactive blue 4 in single and binary systems

Mohammadtaghi Vakili [a,*], Zahra Gholami [b], Babak Salamatinia [c]

[a] Department of Environmental Sciences, College of Agriculture and Environmental Sciences, University of South Africa, Private Bag X06, Florida, 1710, South Africa
[b] Department of Chemistry, Faculty of Science, J. E. Purkyně University in Ústí nad Labem, Pasteurova 15, 400 96, Ústí nad Labem, Czech Republic
[c] Department of Water Services, Metro Vancouver, 4730 Kingsway, Burnaby, BC, Canada

ARTICLE INFO

Keywords:
Chitosan beads
Diepoxyoctane cross-linking
Spermidine functionalization
Hexavalent chromium
Reactive Blue 4
Adsorption isotherms
Binary systems

ABSTRACT

Complex industrial effluents often contain coexisting contaminants that compete for adsorption sites and complicate wastewater treatment. Here, diepoxyoctane-cross-linked and spermidine-functionalized chitosan beads (CHI-DEO-SPD) were developed as acid-stable, amine-rich adsorbents for removing Reactive Blue 4 (RB4) and Cr(VI) from single and binary aqueous systems. The novelty of this strategy lies in combining DEO cross-linking, which improves structural stability under acidic conditions, with spermidine functionalization, which increases the density of protonatable amine sites for anionic pollutant binding. The beads were optimized at 1.5 g/L SPD, 40 °C, and 3 h. FTIR, XRD, TGA, SEM, BET, and pHpzc analyses confirmed successful modification, reduced crystallinity, improved thermal stability, enhanced surface roughness, increased surface area (4.59 to 34.60 m^2/g), and a positively charged surface below pH 6.3. Langmuir capacities reached 872.35 mg/g for RB4 and 785.19 mg/g for Cr(VI) in single-solute systems and remained high in binary systems at 715.26 and 699.92 mg/g, respectively. Kinetic and equilibrium data were best described by pseudo-second-order and Freundlich models, indicating heterogeneous chemisorption driven mainly by electrostatic attraction, hydrogen bonding, and dye-specific π–π interactions. Thermodynamic analysis confirmed spontaneous adsorption in all systems. RB4 adsorption was weakly exothermic in single systems but became endothermic under competition, while Cr(VI) adsorption was endothermic in both systems and more energy-intensive in binary systems. After five regeneration cycles, the beads retained 89.8% and 82.9% of their initial RB4 and Cr(VI) capacities, respectively. These results demonstrate the strong potential of CHI-DEO-SPD beads for treating acidic wastewater containing coexisting dyes and heavy metals.

1. Introduction

Access to clean and safe water remains one of the most pressing challenges of the twenty-first century. Rapid urbanization, industrial expansion, and the widespread discharge of untreated wastewater have severely degraded water quality and threatened public health worldwide. Industries such as textile dyeing and metal processing release hazardous pollutants, including synthetic dyes and heavy metals, into aquatic systems. These contaminants not only disrupt ecosystems but also pose serious risks to human health and compromise the long-term sustainability of water resources [1,2].

Among these pollutants, heavy metals are of particular concern due to their persistence, bioaccumulation, and inherent toxicity [3]. Chromium, widely used in aerospace, leather tanning, chrome plating, and textile industries, exists in multiple oxidation states. Of these, hexavalent chromium (Cr(VI)) is the most problematic because of its high solubility, mobility, and toxicity in aquatic environments [4]. Industrial effluents are a major source of Cr(VI), which has been associated with respiratory disorders, skin lesions, cancers, and even fatalities at low concentrations [5]. The World Health Organization (WHO) classifies Cr(VI) as a Group 1 carcinogen and recommends a maximum permissible concentration of 0.05 mg/L for total chromium in drinking water [4].

Synthetic dyes, particularly reactive dyes, represent another primary class of pollutants in industrial wastewater. These dyes are valued for their stability, bright coloration, and cost-effectiveness, which make them extensively used in textile and electronic applications [6].

* Corresponding author.
E-mail address: mvalili1981@yahoo.com (M. Vakili).

https://doi.org/10.1016/j.ijbiomac.2026.152990
Received 26 February 2026; Received in revised form 29 May 2026; Accepted 8 June 2026
Available online 11 June 2026

However, their high solubility, persistence, and resistance to biodegradation pose serious ecological and health hazards. Their complex aromatic structures contribute to mutagenicity, carcinogenicity, and aquatic toxicity, while also reducing light penetration, increasing biochemical oxygen demand, and enabling bioaccumulation in food chains [7]. Reactive Blue 4 (RB4), in particular, is notoriously resistant to degradation due to its structural complexity and chemical stability [8].

To mitigate these impacts, effective wastewater treatment before discharge is essential. Conventional technologies such as membrane separation, chemical precipitation, coagulation, and oxidation have been applied; however, adsorption has emerged as one of the most efficient and environmentally sustainable alternatives. Adsorption is favored for its simplicity, cost-effectiveness, and the availability of regenerable adsorbents [9,10]. The selection of an appropriate adsorbent is one of the most critical factors for optimizing adsorption performance. Nevertheless, adsorption efficiency strongly depends on the physicochemical properties of both the adsorbent and the target pollutants, highlighting the continuous need for stable, high-capacity, and reusable materials capable of simultaneously removing multiple contaminants [11].

Activated carbon remains the most widely used adsorbent, but its high cost, carbon footprint, and limited regeneration restrict large-scale use [12]. This limitation has driven growing interest in low-cost alternatives derived from agricultural, industrial, and food wastes. Although such materials are eco-friendly and economical, they often display inconsistent adsorption capacities and generally underperform compared with activated carbon [13]. Consequently, natural and renewable materials, particularly biopolymers, have gained attention as sustainable, non-toxic, and versatile adsorbents.

In aqueous systems, the speciation of Cr(VI) depends on both pH and concentration. At concentrations of 0.05–300 mg/L, dihydrogen chromate (H_2CrO_4) predominates at pH < 1, hydrogen chromate ($HCrO_4^-$), and dichromate ($Cr_2O_7^{2-}$) are dominant at pH 1–6, and chromate (CrO_4^{2-}) becomes the main species at pH > 6 [14]. Industrial effluents, particularly from tanning and chromium plating, typically contain Cr (VI) as $HCrO_4^-$ and $Cr_2O_7^{2-}$ due to their highly acidic nature (pH = 2.0–3.0) and high chromium content [15]. Similarly, reactive dyes such as RB4 contain sulfonate groups (–SO_3Na) that dissociate in aqueous solutions to produce negatively charged ions (SO_3^-), conferring strong anionicity [16]. The coexistence of such strongly anionic pollutants underscores the need for positively charged adsorbents capable of effective removal even under acidic conditions.

In industrial wastewater from textile dyeing and metal processing, Cr (VI) and reactive dyes such as RB4 frequently coexist, forming binary or multicomponent systems in which competitive adsorption occurs. Under these conditions, pollutants compete for limited active sites on the adsorbent surface, often resulting in reduced individual removal efficiencies due to antagonistic effects such as site blockage or electrostatic inhibition. For example, studies on grafted chitosan have shown that in mixed systems containing Cr(VI) and reactive dyes such as Remazol Red 3BS, the adsorption capacities of both solutes decrease relative to single-solute systems, with pH exerting a strong influence on selectivity and binding strength [17]. These findings highlight a significant challenge in wastewater treatment, as most adsorbents are optimized for isolated contaminants rather than complex mixtures. Thus, developing materials that sustain high performance in realistic, competitive environments, particularly under acidic conditions typical of industrial effluents, is essential for advancing practical water purification technologies.

Chitosan (CHI), a cationic polysaccharide derived from chitin, has shown considerable promise as an adsorbent due to its low cost, biodegradability, and electrostatic affinity for anionic pollutants. Its cationic character arises from amino groups that become protonated under acidic conditions, enhancing their interaction with negatively charged contaminants. However, CHI's solubility in acidic media limits its practical application, as protonation induces swelling and eventual dissolution [18]. Chemical cross-linking is therefore used to improve mechanical and chemical stability. By forming covalent bonds with functional groups, cross-linking reduces swelling and leaching, increasing acid resistance [19]. Nevertheless, it can also reduce the number of available adsorption sites, potentially lowering adsorption efficiency. The outcome depends on the cross-linker type and degree of modification [18]. Accordingly, research has focused on optimizing cross-linking conditions and introducing additional functional groups with strong affinity for anionic species.

Recent strategies to improve CHI-based adsorbents include grafting quaternary ammonium groups, embedding inorganic nanoparticles (e.g., Fe_3O_4, TiO_2), and cross-linking with agents such as glutaraldehyde or epichlorohydrin [20]. Although these modifications often enhance structural stability and generate new adsorption sites, they can also introduce trade-offs such as reduced biodegradability, increased synthesis complexity, or diminished performance under highly acidic conditions [21]. Moreover, most reported CHI-based adsorbents target either heavy metals or dyes individually, while few have demonstrated simultaneous removal of both classes of pollutants under strongly acidic conditions. Achieving a balance between acidic stability and high adsorption capacity for both Cr(VI) and RB4 remains a significant challenge. Notably, highly reactive cross-linkers such as diepoxyoctane (DEO) have received limited attention, and multifunctional modifications that simultaneously strengthen structural stability and enhance surface amination are rarely optimized for harsh conditions.

To address these limitations, the present study develops a novel CHI-based adsorbent in bead form for the simultaneous removal of Cr(VI) and RB4 under strongly acidic conditions. A central innovation is the use of DEO as a cross-linker, combined with spermidine (SPD) for amino functionalization. DEO, a bifunctional epoxy compound with high aqueous solubility, enables the formation of durable covalent bonds with hydroxyl and amino groups in CHI, thereby enhancing mechanical strength, acid resistance, and adsorption performance [22]. Subsequent functionalization with SPD, a biodegradable polyamine, introduces additional protonatable amino groups, increasing the surface charge density and strengthening electrostatic interactions with anionic contaminants. Compared with conventional chitosan adsorbents, CHI-DEO-SPD beads offer several advantages, including improved acidic stability, enhanced amine density, refined mesoporosity, and strong adsorption affinity toward coexisting anionic contaminants. This design is particularly relevant for acidic industrial effluents, where Cr(VI) oxyanions and sulfonated reactive dyes may coexist and compete for adsorption sites [23].

The effects of SPD concentration, reaction temperature, and functionalization time on adsorption performance were systematically examined. The resulting amino-functionalized, cross-linked beads (CHI-DEO-SPD) were characterized using X-ray diffraction (XRD), thermogravimetric analysis (TGA), scanning electron microscopy (SEM), and Brunauer–Emmett–Teller (BET) analysis. Fourier-transform infrared spectroscopy (FTIR) confirmed functional group modification. Key operational parameters, including initial adsorbate concentration, contact time, pH, and adsorbent dosage, were optimized, and regeneration experiments assessed reusability. Adsorption kinetics and isotherm models were applied to evaluate performance in both single and binary systems. The results demonstrate that CHI-DEO-SPD beads exhibit remarkable structural stability, adsorption capacity, and reusability under strongly acidic conditions, making them highly effective for treating complex industrial wastewater such as that generated by textile dyeing and chrome plating.

2. Materials and methods

2.1. Materials

Analytical-grade reagents were used throughout this study to ensure high purity and eliminate the need for additional purification steps. The

primary chemicals included spermidine (SPD, 98% purity), medium-molecular-weight chitosan (CHI) with a degree of deacetylation of 75–85%, and 1,2,7,8-diepoxyoctane (DEO, 97% purity), all obtained from Sigma–Aldrich. Epichlorohydrin (ECH) and acetone were purchased from Sinopharm Chemical Reagent Co. Sodium hydroxide (NaOH), acetic acid, and potassium chromate were supplied by Beijing Chemical Works. All reagents were used as received without further purification, and deionized (DI) water was used in all experiments.

2.2. Synthesis of amino-functionalized cross-linked chitosan beads

The synthesis of CHI beads began by dispersing 1.5 g of CHI flakes into 100 mL of 1.0% (v/v) acetic acid solution. The mixture was stirred continuously at 25 °C and 400 rpm for 5 h to obtain a homogeneous solution. The resulting CHI solution was then added dropwise to 500 mL of 2 mol/L NaOH using a 10 mL syringe, facilitating bead formation and neutralizing residual acetic acid. The formed beads were washed thoroughly with DI water until the pH reached neutrality, confirming complete removal of excess NaOH.

To prepare cross-linked CHI beads (CHI-DEO), all the neutralized beads (≈15.0 g) were immersed in 200 mL of a 6 g/L DEO solution, adjusted to pH 10. The suspension was agitated in a water bath at 50 °C and 100 rpm for 5 h. After cross-linking, the beads were rinsed several times with DI water to remove unreacted DEO and stored in DI water until further use.

For amino-functionalization, a two-step coupling process was used to immobilize SPD moieties. First, the CHI-DEO beads were activated by reaction with ECH. The beads were immersed in 200 mL of acetone, and 5 mL of ECH was added. The mixture was mechanically stirred at 50 °C for 24 h to promote activation. In this step, ECH acts as a coupling agent, reacting with the hydroxyl and/or amine groups on the CHI-DEO surface to introduce reactive epoxy/chlorohydrin terminals. Subsequently, SPD was covalently attached through these reactive sites. A defined concentration of SPD (0.5–3 mg/L) was gradually introduced to the reaction mixture. Stirring continued for 7 h at temperatures up to 80 °C to facilitate the nucleophilic ring-opening/addition reaction between the primary amines of SPD and the ECH-derived terminals. This step results in the covalent incorporation of SPD molecules into the bead matrix, significantly increasing the surface amine density. After completion, the functionalized beads (denoted CHI-DEO-SPD) were cooled, and thoroughly washed with DI water to remove any residual ECH or SPD. Finally, the product was oven-dried at 50 °C for 24 h to yield CHI-DEO-SPD beads. The synthesis procedure is summarized in Fig. 1.

2.3. Characterization

The effects of cross-linking and functionalization on the physicochemical properties of CHI-DEO-SPD beads were evaluated using multiple analytical techniques. Molecular characteristics were investigated using FT-IR spectroscopy on an FT-IR NEXUS instrument to confirm chemical modifications. Crystallographic characteristics were analyzed via XRD using a Rigaku D/Max RB X-ray diffractometer (Tokyo, Japan). Specific surface area, pore volume, and pore-size distribution were determined using a gas adsorption analyzer (Autosorb-iQ, Quantachrome, USA) by the BET method. Thermal stability was assessed using a TGA/DSC 1 STAR System (Mettler Toledo, USA). Additionally, the surface morphology of the beads was examined using SEM (Merlin Compact, Japan).

The surface charge characteristics were determined using the pH-drift method. A series of 100 mL Erlenmeyer flasks containing 50 mL of 0.05 M NaCl solution (as the background electrolyte) was prepared, and the initial pH ($pH_{Initial}$) was adjusted between 2 and 10 using 0.1 M HCl or 0.1 M NaOH. Subsequently, 20 mg of CHI-DEO-SPD beads were added to each flask, and the suspensions were agitated at 150 rpm for 24 h at 25 ± 1 °C to reach equilibrium. After equilibration, the final pH (pH_{Final}) was measured. The point of zero charge (pHpzc) was determined by plotting $\Delta pH = (pH_{Final} - pH_{Initial})$ against $pH_{Initial}$. The pHpzc corresponds to the point where $\Delta pH = 0$, indicating electrostatic neutrality of the adsorbent surface.

2.4. Adsorption experiments

Batch adsorption experiments were conducted for both single-solute and binary-solute systems to assess the adsorption performance of CHI-DEO-SPD beads for RB4 and Cr(VI) removal. Each test was performed in 100 mL Erlenmeyer flasks containing 50 mL of adsorbate solution (RB4, Cr(VI), or both) and a defined dosage of CHI-DEO-SPD beads. The flasks were agitated at 180 rpm on an orbital shaker at a constant temperature of 25 °C. To optimize adsorption performance, key parameters were systematically varied, including adsorbent dosage (0.25–1.5 g/L), contact time (up to 24 h), initial adsorbate concentration (50–300 mg/L), and solution pH (3–11). In single-solute systems, only one contaminant (RB4 or Cr(VI)) was present, while in binary systems, both were introduced at equal initial concentrations. All experiments were performed in triplicate to ensure reproducibility and statistical reliability.

At equilibrium, the CHI-DEO-SPD beads were separated from the solutions, and the supernatant was analyzed to determine residual concentrations. UV–visible spectrophotometry (Hach DR 5000) was employed at 599 nm for RB4 and 540 nm for Cr(VI). The adsorption capacity (q_e) and removal efficiency (R%) were calculated using Eqs. (1) and (2), respectively. Kinetic experiments were conducted at an initial adsorbate concentration of 100 mg/L (pH 3, 25 °C) for both systems. Aliquots were collected at predetermined time intervals over a 24 h period, and the data were fitted to pseudo-first-order (PFO) and pseudo-

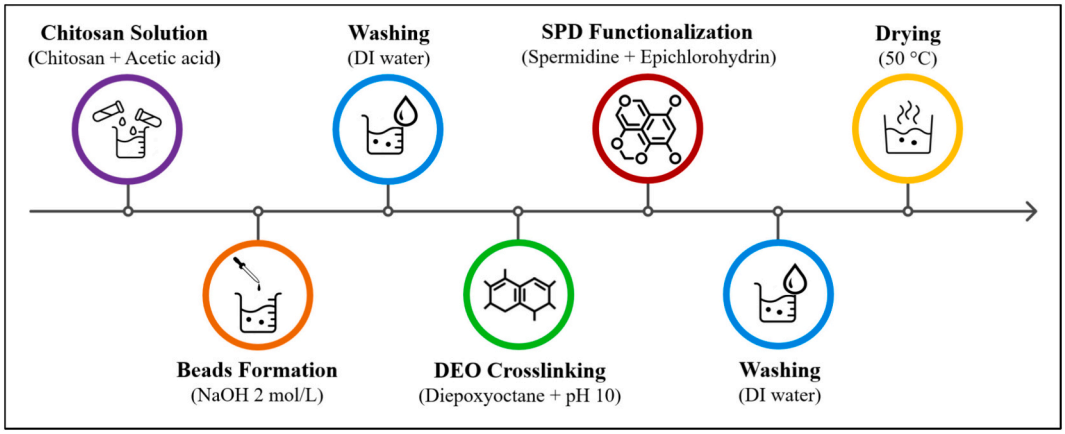

Fig. 1. Schematic representation of the CHI-DEO-SPD beads synthesis process.

second-order (PSO) models (Eqs. (3) and (4)). The Elovich model (Eq. (5)) was also applied to provide additional insight into the adsorption mechanism and surface heterogeneity.

Isotherm experiments were performed at pH 3 with six initial concentrations (50–300 mg/L) and three temperatures (25, 35, and 45 °C). The equilibrium data for both single- and binary-systems were analyzed using the Langmuir and the Freundlich models (Eqs. (6) and (7)). Model accuracy was evaluated by the chi-square (χ^2) error function (Eq. (8)). Thermodynamic parameters, including Gibbs free energy change (ΔG^0), enthalpy change (ΔH^0), and entropy change (ΔS^0), were calculated from the temperature dependence of Langmuir constants using the van't Hoff equations (Eqs. (9) and (10)) [24].

$$q_e = \frac{(C_0 - C_e) \times V}{m} \tag{1}$$

$$R\% = \frac{(C_0 - C_e)}{C_0} \times 100 \tag{2}$$

$$q_t = q_e\left(1 - e^{-K_1 t}\right) \tag{3}$$

$$q_t = \frac{K_2 q_e^2 t}{1 + K_2 q_e t} \tag{4}$$

$$q_t = \frac{1}{\beta}\ln(\alpha\beta t) \tag{5}$$

$$q_e = \frac{q_m C_e b}{1 + bC_e} \tag{6}$$

$$q_e = K_F C_e^{\,1/n} \tag{7}$$

$$\chi^2 = \sum \frac{\left(q_{e,exp} - q_{e,\ cal}\right)^2}{q_{e,cal}} \tag{8}$$

$$\Delta G^\circ = -RT\ln(b) \tag{9}$$

$$\ln(b) = \frac{\Delta S^\circ}{R} - \frac{\Delta H^\circ}{RT} \tag{10}$$

In these equations, q_e and q_t (mg/g) represent the adsorption capacities at equilibrium and at a given time t, respectively. C_0 and C_e (mg/L) denote the initial and equilibrium adsorbate concentrations. V (L) is the adsorbate solution volume, and m (g) is the dry mass of the adsorbent. R% indicates the percentage removal efficiency. For the kinetic models K_1 (h^{-1}) and K_2 (g/(mg.h)) are the rate constants for the pseudo-first-order (PFO) and pseudo-second-order (PSO) models, respectively, while t (min) is the contact time. Also, α (mg/g·h) is the initial adsorption rate, and β (g/mg) is the desorption constant related to surface heterogeneity. In the Langmuir isotherm, q_m (mg/g) is the maximum monolayer adsorption capacity, and b (L/mg) is the Langmuir constant, which reflects the affinity of the adsorbent for the adsorbate. The Freundlich constants K_F ((mg/g)(mg/L)$^{1/n}$) and n (dimensionless), describe the adsorption capacity and intensity, respectively. The calculated adsorption capacity obtained from model fitting is denoted as q_{cal} (mg/g) and χ^2 represents the chi-square statistic used to evaluate the goodness of fit between experimental and modeled data. Finally, R is the universal gas constant (8.314×10^{-3} kJ/mol/K), and T is the absolute temperature in Kelvin (K).

2.5. Reusability study

The regeneration performance of CHI-DEO-SPD beads was assessed through consecutive adsorption–desorption cycles. For adsorption, the beads were immersed in 100 mL of aqueous solution containing 100 mg/L of RB4 dye and 100 mg/L of Cr(VI) ions. The suspension was agitated at 180 rpm and maintained at 25 °C with the solution pH adjusted to 3 for 24 h to ensure equilibrium adsorption. Afterward, the beads were separated and thoroughly rinsed with DI water to remove unbound species. Desorption was performed by transferring the loaded beads into 100 mL of 1.0 mol/L NaOH solution, followed by agitation at 180 rpm and 25 °C for 2 h. The alkaline environment promoted desorption by deprotonating amino groups and disrupting electrostatic interactions between the cationic adsorbent and anionic pollutants. After desorption, the beads were repeatedly rinsed with DI water until the rinse water reached neutral pH, ensuring removal of residual NaOH and desorbed solutes. The adsorbent was then dried in an oven at 50 °C overnight before reuse. This adsorption–desorption process was repeated multiple times to evaluate reusability. The adsorption efficiency of the regenerated beads was determined after each cycle, and experiments continued until a marked decline in performance was observed. The progressive decrease in removal efficiency with repeated cycles was used to assess the stability and long-term applicability of the CHI-DEO-SPD beads for repeated wastewater treatment operations.

2.6. Statistical analysis

All optimization experiments were performed in triplicate, and results were expressed as mean ± standard deviation. One-way analysis of variance (ANOVA) was employed to determine the statistical significance of synthesis parameters (SPD concentration, reaction time, and temperature) on RB4 removal efficiency. When ANOVA indicated significant differences ($p < 0.05$), Tukey's honestly significant difference (HSD) post-hoc test was performed for multiple comparisons between individual groups. All statistical analyses were carried out using OriginPro 2021 (OriginLab Corporation, Northampton, MA, USA).

3. Results and discussion

3.1. Optimizing SPD functionalization conditions

Optimizing key parameters during the functionalization process is critical to maximizing the adsorption capacity of CHI-DEO-SPD beads. These parameters include SPD concentration, functionalization duration, and temperature. Proper adjustment of these factors significantly enhances the performance of CHI-DEO-SPD beads in adsorption applications. RB4 was selected as the model anionic dye for optimization due to its structural complexity and sulfonic acid groups, which make it representative of many anionic contaminants in wastewater. It was preferred over Cr(VI) because it is safer to handle, allows rapid concentration measurements by UV–Vis spectrophotometry, and enables high-throughput testing. In contrast, Cr(VI) requires strict safety protocols, generates hazardous waste, and needs more time-consuming analyses. Both RB4 and Cr(VI) are anionic under acidic conditions and interact with cationic sites on beads through similar electrostatic mechanisms. Therefore, RB4 was chosen as a practical surrogate for determining adsorption conditions. These conditions were subsequently validated for Cr(VI) removal. To statistically validate the optimization ANOVA was performed for each synthesis parameter using triplicate experimental data (Table 1), followed by Tukey's honestly significant difference (HSD) post-hoc test to identify significant differences between specific levels.

3.1.1. Effect of reaction time

Fig. 2a illustrates the adsorption behavior of RB4 dye onto CHI-DEO-SPD beads prepared with varying reaction times (1–7 h). The data revealed that RB4 uptake follows a distinct pattern: initially, adsorption efficiency increased rapidly, reaching a maximum within the first 3 h. Specifically, the adsorption efficiency improved from 57.76% at 1 h to 64.99% at 3 h. This increase is likely due to the prolonged interaction between the CHI-DEO beads and SPD, which facilitates a greater binding of SPD molecules to the functional groups on the CHI-DEO surface. As more SPD molecules are attached, the density of amino functional

Table 1
ANOVA results for optimization of CHI-DEO-SPD synthesis parameters.

Factor	Source	Sum of squares	df	Mean square	F-value	p-Value
A: Reaction time	Model	128.47	6	21.41	98.67	<0.0001
	Error	3.04	14	0.22		
	Total	131.51	20			
B: Temperature	Model	5334.67	6	889.11	1965.8	<0.0001
	Error	6.33	14	0.45		
	Total	5341.00	20			
C: SPD concentration	Model	4979.42	6	829.90	2369.5	<0.0001
	Error	4.90	14	0.35		
	Total	4984.32	20			

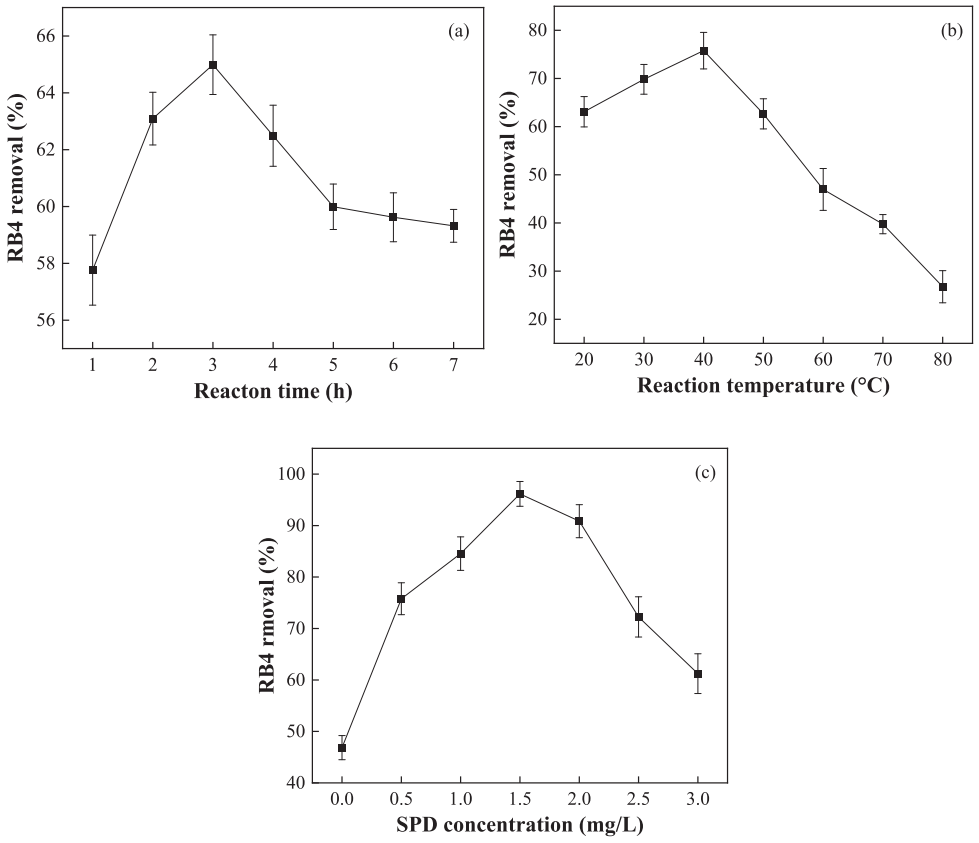

Fig. 2. Effect of functionalization parameters: time (a), temperature (b), and SPD concentration (c), on RB4 uptake by CHI-DEO-SPD beads (0.5 g/L CS-DEO-SP beads in 100 mL of 30 mg/L RB4 solution for 24 h at room temperature).

groups on the adsorbent surface increases, thereby enhancing the RB4 adsorption capacity [15]. However, beyond this initial phase, the efficiency of RB4 removal gradually declined, reaching a minimum of 59.3% after 7 h. This decline suggests that the functional sites on the CHI-DEO surface became saturated. As a result, fewer active sites remained available, and the concentration of free SPD molecules in solution decreased. Consequently, extending the reaction time beyond this point did not improve RB4 adsorption, indicating that additional reaction time was ineffective in enhancing adsorption performance. ANOVA confirmed that reaction time had a statistically significant effect on RB4 removal ($F(6,14) = 98.67$, $p < 0.0001$). Post-hoc Tukey HSD tests revealed that 3 h yielded significantly higher removal than all other times tested ($p < 0.05$). These results confirm that extending the reaction time beyond 3 h was ineffective and even detrimental to adsorption performance.

3.1.2. *Effect of temperature*

The effect of temperature on RB4 adsorption by CHI-DEO-SPD beads was also investigated, with synthesis temperatures ranging from 20 °C to 80 °C. As shown in Fig. 2b, increasing the temperature initially enhanced RB4 adsorption; however, further increases in temperature resulted in a decline in adsorption efficiency. The adsorption efficiency peaked at 40 °C, achieving a removal rate of 75.7%. This improvement is attributed to the increased kinetic energy of SPD molecules at elevated temperatures, which accelerates the reaction rate between CHI-DEO and SPD. The enhanced molecular motion and energy of SPD molecules result in more frequent and effective collisions between reactant molecules, thereby increasing the likelihood of successful product formation [25].

Nevertheless, as the temperature increased to 80 °C, the RB4 removal efficiency declined sharply to just 26.7%. This decrease can be explained by several interrelated factors, including the disruption of hydrogen bonding between the adsorbent and SPD molecules, thermal degradation of the chitosan backbone, and the resulting loss of structural integrity and adsorption capacity at elevated temperatures. At such high synthesis temperatures, SPD (a linear polyamine) may undergo oxidative deamination and intramolecular cyclization. These reactions yield degradation products that lack the primary amine groups required for

strong electrostatic interactions with RB4. In parallel, chitosan is susceptible to heat-induced depolymerization and deacetylation, leading to chain scission and a reduction in molecular weight. Meanwhile, Maillard-type condensation between SPD amino groups and oxidized chitosan carbonyls can form Schiff base linkages that block protonatable sites. Excess thermal energy may also disrupt the hydrogen-bonding network within the chitosan matrix, lowering crystallinity, decreasing surface area, and reducing the number of accessible adsorption sites. Collectively, these degradation and side-reaction pathways reduce both the net positive charge density and the structural stability of the CHI-DEO-SPD beads, ultimately impairing their adsorption performance [26,27]. ANOVA demonstrated a highly significant effect of temperature on RB4 removal ($F(6,14) = 1965.8$, $p < 0.0001$). Tukey HSD analysis confirmed that 40 °C provided significantly higher removal than all other temperatures tested ($p < 0.0001$).

3.1.3. Effect of SPD concentration

The influence of SPD concentration on RB4 adsorption was examined (Fig. 2c). The results indicate that increasing SPD concentration initially enhanced RB4 removal efficiency, reaching a maximum at 1.5 g/L. This significant enhancement in adsorption, which increased from 46.85% to 96.15%, is likely due to the increased availability of amino functional groups on the CHI-DEO-SPD bead surfaces resulting from the incorporation of more SPD during synthesis. These functional groups provide additional active sites for RB4 adsorption [15]. However, increasing SPD concentration beyond 1.5 g/L decreased RB4 removal efficiency, dropping to 61.23% at 3.0 g/L. This reduction is likely due to saturation of adsorption sites, which may cause steric hindrance, limiting RB4 accessibility. Therefore, achieving optimal RB4 adsorption on CHI-DEO-SPD beads requires careful control of SPD concentration during bead synthesis to avoid exceeding the threshold at which additional SPD becomes counterproductive. ANOVA confirmed that SPD concentration had a statistically significant effect on RB4 removal ($F(6,14) = 2369.5$, $p < 0.0001$). Post-hoc Tukey HSD tests revealed that 1.5 g/L SPD yielded significantly higher removal than all other concentrations tested ($p < 0.0001$), including 1.0 g/L (84.57%) and 2.0 g/L (90.87%). Based on the statistical analysis, the optimal functionalization conditions were confirmed as: 1.5 g/L SPD, 40 °C, and 3 h reaction time. These conditions were used for subsequent characterization and adsorption studies.

3.2. Characterization

The FTIR spectrum of pristine CHI beads displayed characteristic absorption bands attributable to chitosan functional groups (Fig. 3a). A broad band between 3100 and 3600 cm^{-1} was assigned to the stretching vibrations of hydroxyl (−OH) and amine ($-NH_2$) groups, both typical of chitosan. The peak at 2871 cm^{-1} corresponded to C—H stretching in aliphatic $-CH_2$ groups [28]. Distinct bands observed at 1658, 1590, 1552, and 1311 cm^{-1} were attributed, respectively, to amide I (C═O stretching), the overlapping N—H bending of primary amines with amide II contributions, and C—N stretching coupled with N—H bending for amide III [29]. Peaks at 1417 and 1371 cm^{-1} were assigned to C—H bending and the symmetric deformation of $-CH_3$ groups [30]. The band at 1143 cm^{-1} corresponded to the asymmetric stretching of C–O–C bridges in glycosidic linkages, whereas those at 1058 and 1022 cm^{-1} were associated with C—O stretching of the saccharide backbone, features characteristic of CHI [29].

In contrast, the FTIR spectrum of CHI-DEO-SPD beads exhibited clear band shifts and intensity changes consistent with successful cross-linking and amine functionalization. The overlapping $-NH_2$ and −OH

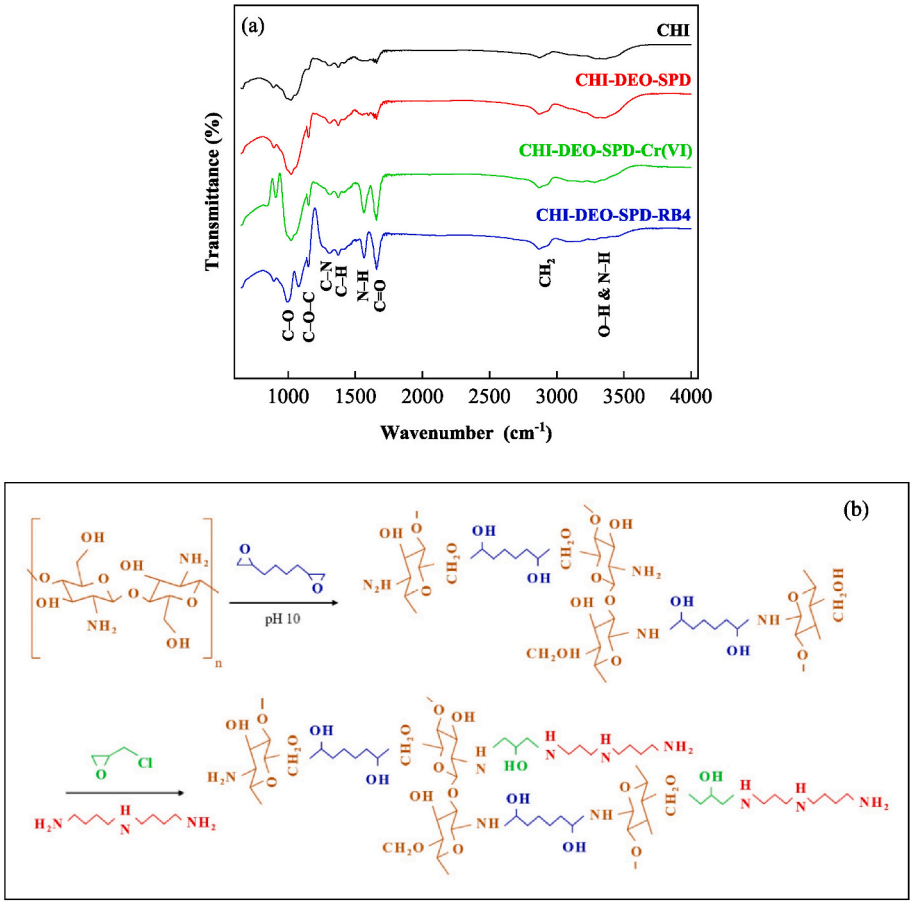

Fig. 3. FT-IR spectra of CHI and CHI-DEO-SPD beads before and after adsorption (a), and schematic illustration of the CHI-DEO-SPD bead synthesis process (b).

stretching band (3350 cm^{-1}) intensified and broadened, indicating enhanced hydrogen bonding and an increased population of amine groups from the incorporated SPD [31]. The C—H stretching region near 2860 cm^{-1} also changed in intensity, reflecting modifications to the CHI matrix and the incorporation of new groups.

Importantly, the interpretation of reactive group formation was refined. The amide I band shifted from 1658 cm^{-1} to 1661 cm^{-1}, and the complex band at ~1590 cm^{-1} (encompassing N—H bending/amide II) shifted to 1596 cm^{-1}. These shifts signify an altered chemical environment for the carbonyl and amine groups, consistent with their involvement in reactions with DEO and ECH, and the subsequent introduction of SPD [32]. Crucially, the C–O–C/C–O stretching region showed a notable shift from 1058 cm^{-1} to 1151 cm^{-1}. This shift toward higher wavenumbers is a key indicator of the formation of new aliphatic ether (C–O–C) linkages, which is the expected product of the ring-opening reactions of DEO and ECH epoxides with chitosan's hydroxyl and amine groups [15]. Collectively, these spectral changes confirm: (1) the formation of a cross-linked network via DEO/ECH, and (2) the successful incorporation of SPD amines, resulting in a material with higher amine density and structural stability. Fig. 3b schematically illustrates the proposed DEO cross-linking and SPD attachment on the CHI surface.

Fig. 4a presents the XRD patterns of CHI and CHI-DEO-SPD beads. The CHI beads exhibited two distinct characteristic reflections: a broad, weak feature near 11° and a more intense, sharper peak at 20.24°. These are well-known signatures of semi-crystalline chitosan; the low-angle reflection is commonly associated with hydrated, less-ordered crystalline domains, whereas the 20° reflection corresponds to more ordered, anhydrous/semi-crystalline regions [33]. Together they confirm the semi-crystalline nature of CHI, which arises primarily from extensive inter- and intra-chain hydrogen bonding involving hydroxyl and amine groups [34].

After cross-linking with DEO and functionalization with SPD, the XRD patterns exhibited substantial changes. The overall intensity of the diffraction peaks decreased, and the reflection at 20.24° shifted slightly to 20.56°, accompanied by noticeable peak broadening. These alterations indicate a partial loss of crystallinity and an increase in amorphous content, suggesting that cross-linking and grafting disrupted the regular hydrogen-bonding network of CHI [35]. The reduction in crystallinity can be attributed to the insertion of DEO and SPD between CHI polymer chains, which hinders tight packing and introduces structural disorder. Although reduced crystallinity may slightly compromise rigidity, it increases the accessibility of internal functional groups to adsorbates and enhances flexibility, both of which are favorable for adsorption. Consequently, CHI-DEO-SPD beads exhibit higher adsorption efficiency due to improved surface accessibility and expanded diffusion pathways [36].

TGA provided further insight into the thermal stability and decomposition behavior of the synthesized adsorbents (Fig. 4b). The thermogram of pristine CHI beads exhibited three distinct weight-loss stages. The first stage, occurring near 100 °C (approximately 4.0% mass loss), corresponds to the desorption of physically adsorbed and bound water from the hydrophilic CHI matrix [37]. The major decomposition occurred between 250 and 450 °C, resulting in substantial mass loss primarily due to the depolymerization and degradation of the chitosan backbone, which involves the dehydration of saccharide units and the cleavage of acetylated and deacetylated moieties [38]. Beyond 550 °C, further decomposition occurred, leaving a residual char of 4.5%, indicative of the limited thermal stability of unmodified CHI.

In contrast, CHI-DEO-SPD beads exhibited enhanced thermal stability and a modified decomposition pattern. The initial weight loss below 120 °C decreased to 2.64%, indicating reduced water retention due to cross-linking, which limits the availability of highly hydrophilic sites [39]. The primary decomposition proceeded in two overlapping stages: an initial mass loss of 43.65% between 290 and 340 °C, followed by a second stage between 450 and 500 °C, yielding a total mass loss of 74% over these temperature ranges. This two-step degradation pattern suggests structural complexity introduced by DEO cross-linking and SPD grafting, leading to decomposition of distinct molecular domains at different temperatures [38]. At 550–600 °C, CHI-DEO-SPD beads exhibited a total mass loss of 91.8%, corresponding to a residual char yield of 8.2%, nearly double that of pristine CHI. The higher char residue indicates the formation of thermally stable carbonaceous structures reinforced by covalent cross-links and polyamine moieties. This improvement confirms that DEO cross-linking and SPD incorporation strengthen the CHI framework, delay degradation, and enhance suitability for applications under harsh thermal or acidic conditions.

The pore structure and surface area play critical roles in adsorption performance, influencing both the accessibility of active sites and the diffusion of adsorbates. BET analysis results for CHI and CHI-DEO-SPD beads are summarized in Table 2. Following modification, substantial increases in surface area and total pore volume were observed, accompanied by a reduction in average pore diameter. Quantitatively, the BET surface area increased from 4.59 m^2/g for pristine CHI to 34.60 m^2/g after modification (an almost eightfold increase). Similarly, the total pore volume rose from 0.03 cm^3/g to 0.09 cm^3/g, while the average pore diameter decreased from 31.50 nm to 11.01 nm. According to IUPAC classification, both materials are mesoporous (2–50 nm); the modification thus led to a refinement of the mesoporous structure, generating a higher population of pores in the smaller mesopore range [40]. These

Table 2
Textural characteristics of CHI and CHI-DEO-SPD beads.

Adsorbent	BET surface area (m^2/g)	Total pore volume (cm^3/g)	Average pore diameter (nm)
CHI	4.59	0.03	31.50
CHI-DEO-SPD	34.60	0.09	11.01

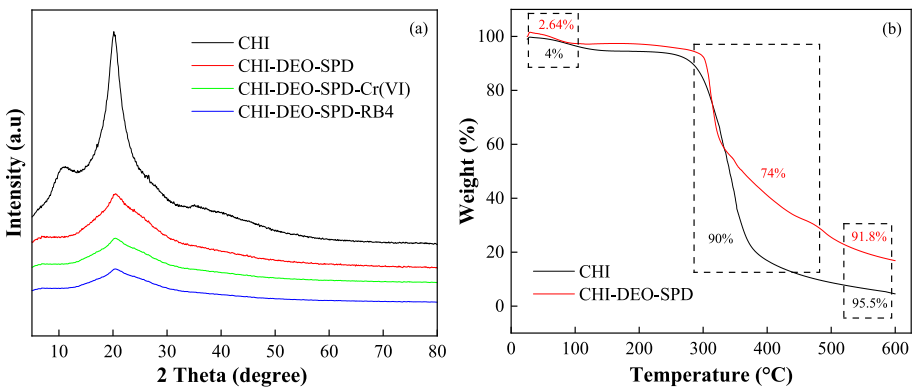

Fig. 4. XRD patterns (a), and TGA curves (b) of the CHI and CHI-DEO-SPD beads.

results confirm that DEO cross-linking and SPD functionalization introduced structural rearrangements, generating additional mesoporosity and improving access to adsorption sites. The shift to a smaller average pore diameter (~11 nm) indicates the creation of a more defined mesoporous network. This pore size is highly relevant for the adsorption of large organic molecules, such as dyes (e.g., RB4), while remaining readily accessible to smaller inorganic ions, such as Cr(VI) oxyanions. The improvement in surface properties is mainly attributed to partial disruption of dense chitosan networks, followed by cross-linking that stabilizes the network and prevents collapse during drying, which generated a more open and interconnected pore system. The grafted amino groups also increase molecular spacing and enhance structural porosity. Consequently, CHI-DEO-SPD beads combine high surface area, appropriate mesopore size, and abundant active sites, making them highly effective for simultaneous adsorption of dyes and metal ions.

SEM analysis was performed to examine the morphological characteristics of the synthesized beads (Fig. 5). The images reveal that pristine CHI beads exhibit a smooth, uniform, and relatively compact surface morphology. In contrast, CHI-DEO-SPD beads display a rougher and more irregular surface texture, indicating a heterogeneous and porous structure. These morphological transformations result from modification with DEO and SPD, which alter surface topography and increase the number of accessible functional groups. The rough, heterogeneous surface of CHI-DEO-SPD enhances the availability of active sites and promotes stronger interactions with adsorbates. Consequently, these structural changes improve adsorption efficiency and confirm the successful modification of CHI beads.

3.3. Effect of adsorbent dosage

Determining the optimal adsorbent dosage is essential to maximize removal efficiency while maintaining cost-effectiveness and minimizing material use. In adsorption systems, the adsorbent dosage directly influences the number of available active sites, the degree of adsorbate–adsorbent contact, and the overall driving force for mass transfer between the solid and liquid phases [41]. The results revealed that increasing the dosage of CHI-DEO-SPD beads markedly enhanced the removal of both RB4 and Cr(VI) in single- and binary-solute systems up to an optimal concentration of 1.0 g/L, beyond which no significant improvement was observed (Fig. 6a). As expected, the adsorption efficiencies in the binary system were consistently lower than those in the single-solute experiments, reflecting the competitive nature of co-adsorption.

In the single-solute systems, the removal efficiencies of both contaminants increased sharply as the adsorbent dosage rose from 0.25 to 1.0 g/L. For Cr(VI), the removal efficiency improved from 30.05% to 73.00%, while RB4 removal increased from 42.05% to 85.00%. This enhancement in performance at higher dosages can be attributed to the greater surface area and larger number of active sites available for adsorption, enabling more effective interactions between the functional groups on the CHI-DEO-SPD surface and the adsorbate molecules [42]. Under acidic conditions (pH 3), the positively charged amino groups ($-NH_3^+$) on the CHI-DEO-SPD surface play a dominant role in attracting negatively charged species through electrostatic interactions. Both RB4 dye anions (bearing sulfonate groups, $-SO_3^-$) and Cr(VI) oxyanions ($HCrO_4^-$ and $Cr_2O_7^{2-}$) are effectively drawn toward these protonated amine sites. In addition to electrostatic attraction, secondary mechanisms, such as hydrogen bonding and π–π interactions between the aromatic rings of RB4 and the chitosan backbone, contribute to dye adsorption. This combination of interactions explains the consistently higher RB4 removal efficiency compared with Cr(VI), as the latter depends almost exclusively on electrostatic binding.

Beyond the optimal dosage of 1.0 g/L, the removal efficiency plateaued and even declined slightly at higher dosages. This behavior is commonly attributed to the aggregation of adsorbent particles, which reduces the effective surface area and partially blocks active sites, thereby lowering the overall adsorption capacity. Additionally, at elevated bead concentrations, the overlapping of diffusion layers surrounding adjacent particles can hinder the mass transfer of adsorbate molecules from the bulk solution to the adsorbent surface, reducing apparent efficiency [43].

A similar trend was observed in the binary-solute system, although overall efficiencies were lower due to competition for shared adsorption

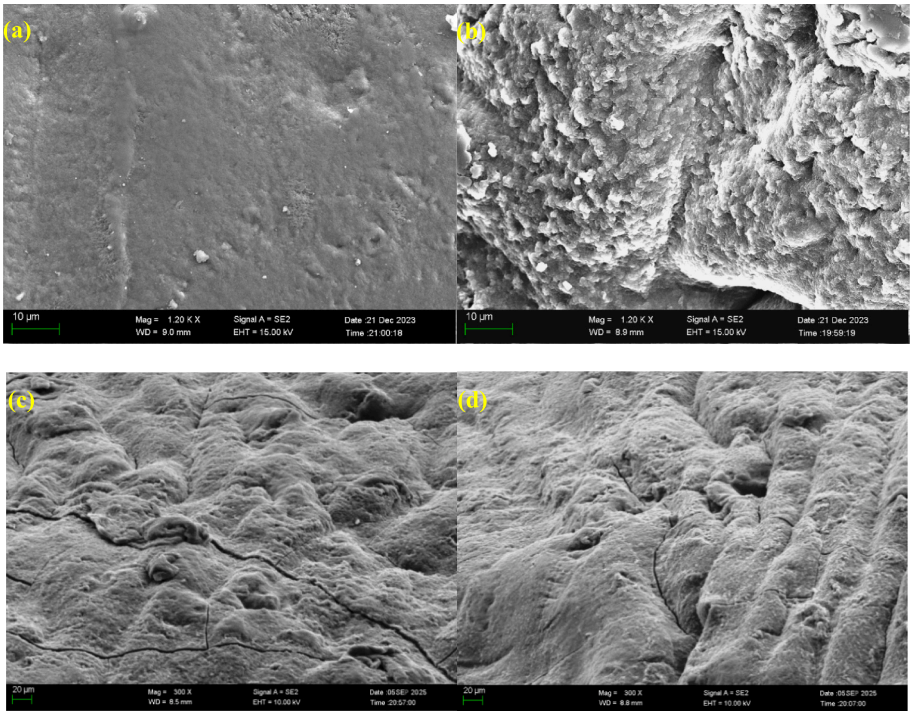

Fig. 5. SEM images of CHI beads (a), CHI-DEO-SPD beads (b), CHI-DEO-SPD after RB4 adsorption (c), and CHI-DEO-SPD after Cr(VI) adsorption (d).

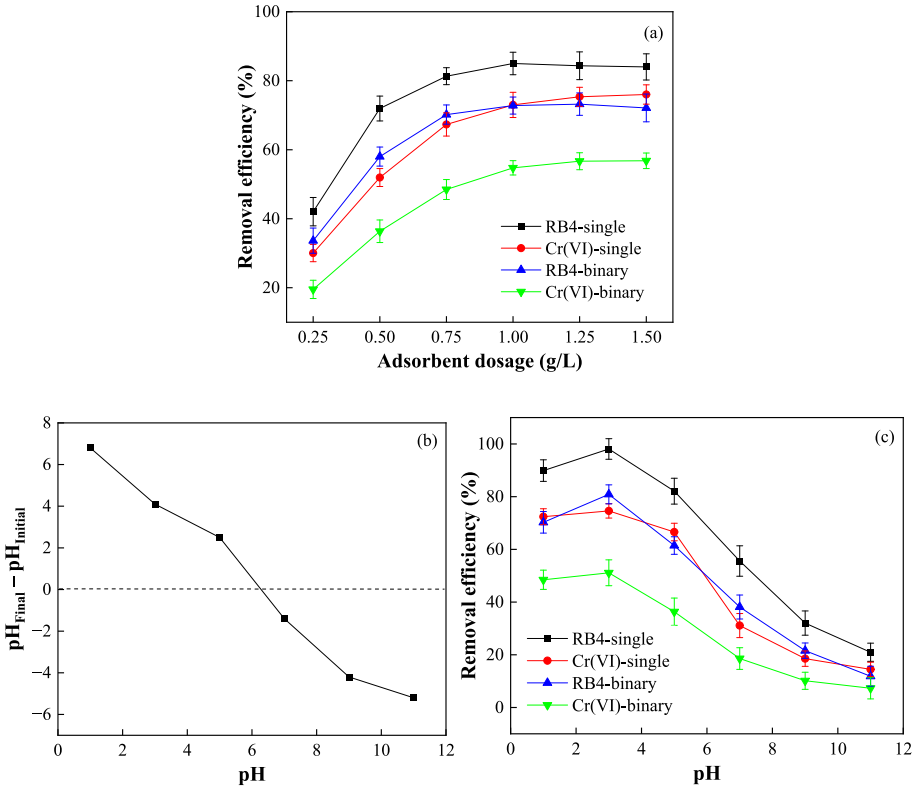

Fig. 6. Effect of adsorbent dosage (a), point of zero charge (b), and initial pH (c) on the adsorption of RB4 and Cr(VI) onto CHI-DEO-SPD beads in single- and binary-solute systems (100 mL solution; 50 mg/L for single-solute; 50 + 50 mg/L for binary-solute; 24 h, room temperature).

sites. RB4 removal increased from 33.64% at 0.25 g/L to 72.80% at 1.0 g/L, after which it stabilized. Cr(VI) removal rose from 19.53% at 0.25 g/L to 57.80% at 1.5 g/L, remaining consistently below single-solute values. The reduced performance in the binary system reflects the strong competitive adsorption between RB4 and Cr(VI), as both anionic species vie for the same positively charged sites. Despite this competition, RB4 exhibited a greater affinity for CHI-DEO-SPD beads than Cr (VI), even under mixed conditions. This preferential adsorption arises from RB4's ability to participate in multiple binding mechanisms, including electrostatic attraction, hydrogen bonding, and π–π stacking interactions, whereas Cr(VI) relies mainly on electrostatic forces. Moreover, the larger molecular size and conjugated aromatic structure of RB4 enable multilayer adsorption and surface occupation at multiple binding sites, providing a kinetic advantage in accessing available active sites. Overall, these results demonstrate that an adsorbent dosage of 1.0 g/L provides the best balance between high removal efficiency and material economy. This dosage ensures sufficient availability of active sites while minimizing the negative effects of aggregation and diffusion limitation. Therefore, 1.0 g/L was selected as the optimal adsorbent dosage for subsequent kinetic, isotherm, and thermodynamic investigations.

3.4. Effect of pH

Determining the pHpzc of an adsorbent provides valuable insight into its surface chemistry, adsorption behavior, and dominant interaction mechanisms. The pHpzc is the pH at which the adsorbent's net surface charge is zero. When pH > pHpzc, the surface becomes negatively charged, favoring the adsorption of cationic species. Conversely, when pH < pHpzc, the surface is positively charged, enhancing the uptake of anionic pollutants such as Cr(VI) oxyanions and sulfonated dye molecules [44].

As shown in Fig. 6b, the surface charge of CHI-DEO-SPD beads was strongly influenced by the solution pH. The experimentally determined pHpzc was 6.3, indicating that the bead surface is positively charged below this value and negatively charged above it. Thus, at pH < 6.3, electrostatic attraction occurs between protonated amino groups ($–NH_3^+$) on the adsorbent and negatively charged Cr(VI) and RB4 species, promoting efficient adsorption. This explains the high removal efficiencies observed under acidic conditions, with optimal performance at pH 2–3. In contrast, at pH > 6.3, deprotonation of surface amino groups reduces the positive surface charge and induces electrostatic repulsion toward anionic contaminants, leading to a pronounced decline in adsorption efficiency.

The pH of the solution plays a pivotal role in controlling both the physicochemical properties of the adsorbent and the speciation of the adsorbate. It governs the protonation and deprotonation of surface functional groups, thereby determining the charge distribution at the solid–liquid interface [45]. Both RB4 and Cr(VI) exist predominantly as anionic species in aqueous media. Deprotonation of sulfonic acid groups ($-SO_3H$) in RB4 generates sulfonate ions ($-SO_3^-$), imparting a strong negative charge to the dye molecule [46]. Similarly, Cr(VI) exists predominantly as oxyanions such as CrO_4^{2-}, $Cr_2O_7^{2-}$, and $HCrO_4^-$, depending on the pH and total concentration. Under acidic conditions (pH < 6), $HCrO_4^-$ and $Cr_2O_7^{2-}$ dominate, whereas CrO_4^{2-} becomes predominant in alkaline media. These negatively charged species interact most effectively with positively charged surfaces [47]. At low pH, the protonation of amino groups ($–NH_2 \rightarrow –NH_3^+$) enhances the positive surface potential of CHI-DEO-SPD beads, resulting in strong electrostatic attraction toward anionic RB4 and Cr(VI) species. Additionally, excess H^+ ions suppress the dissociation of surface hydroxyl groups, further minimizing electrostatic repulsion. Therefore, acidic environments strongly favor adsorption.

Experimental data confirmed this expectation: both RB4 and Cr(VI) removal efficiencies increased substantially at low pH. In single-solute systems, adsorption exhibited a clear pH dependence, with maximum removal efficiencies of 98.08% for RB4 and 74.58% for Cr(VI) at pH 3 (Fig. 6c). At this pH, RB4 exists mainly as RB4–SO_3^-, while Cr(VI) occurs

primarily as $HCrO_4^-$. The extensive protonation of amino groups on CHI-DEO-SPD (forming $-NH_3^+$ sites) facilitates strong electrostatic attraction with these negatively charged species [48].

At pH values below 3, partial protonation of RB4 sulfonate groups to $-SO_3H$ slightly decreases the dye's negative charge; however, RB4 largely retains its anionic character and continues to adsorb effectively. In contrast, under highly acidic conditions, Cr(VI) shifts toward its neutral molecular form, H_2CrO_4, which exhibits a weaker electrostatic affinity for the protonated adsorbent, leading to reduced adsorption [49]. Moreover, excessive protonation of surface amino groups can generate intramolecular electrostatic repulsion and partially neutralize charges, diminishing overall adsorption capacity [50].

As the pH increased from 3 to 11, the adsorption capacities of both RB4 and Cr(VI) decreased sharply, to 20.95% and 14.45%, respectively. This decline results from the deprotonation of amino groups, which reduces positive charge density and induces electrostatic repulsion between the negatively charged adsorbent surface and the anionic adsorbates. In alkaline media, hydroxide ions (OH^-) also compete with Cr(VI) oxyanions and RB4 sulfonates for active sites, further hindering adsorption. Additionally, at high pH, the diminished hydrogen-bonding capacity and potential swelling relaxation of the chitosan framework can slightly reduce surface accessibility [51].

In the binary-solute system, a similar pH-dependent trend was observed, although overall adsorption efficiencies were lower due to competition for available sites [52]. For RB4, the maximum removal efficiency at pH 3 was 80.88%, compared with 98.08% in the single-solute system, while for Cr(VI) it was 51.09%, dropping to 7.28% at pH 11. The stronger suppression of Cr(VI) uptake in the binary system suggests that RB4 possesses a higher affinity for the available cationic sites and effectively outcompetes Cr(VI) under coexisting conditions.

The preferential adsorption of RB4 can be attributed to its multiple binding mechanisms. In addition to electrostatic attraction, RB4 interacts through hydrogen bonding between its sulfonate moieties and the amino or hydroxyl groups on CHI-DEO-SPD, as well as through π–π stacking between its aromatic rings and the polysaccharide backbone. By contrast, Cr(VI) adsorption relies primarily on electrostatic interactions. This structural versatility provides RB4 with both kinetic and thermodynamic advantages, explaining its dominant removal performance under single- and binary-solute conditions [52].

Overall, adsorption of both RB4 and Cr(VI) was most effective under acidic conditions and decreased progressively with increasing pH. However, in multicomponent systems, competitive interactions significantly reduced the uptake of both species, particularly Cr(VI). These results demonstrate that RB4 exhibits a higher affinity toward CHI-DEO-SPD due to its diverse binding modes, while Cr(VI) adsorption is more sensitive to electrostatic competition. This behavior highlights the importance of evaluating adsorption performance under realistic multicomponent conditions, as single-solute studies may overestimate adsorbent efficiency in practical wastewater treatment applications.

3.5. Adsorption kinetics

Contact time is one of the most critical parameters influencing adsorption performance, as it determines the rate at which equilibrium is achieved and reflects the overall efficiency of the adsorbent. Understanding adsorption kinetics is therefore essential for optimizing treatment system design to ensure high removal efficiency and cost-effectiveness [53]. The adsorption of RB4 and Cr(VI) onto CHI-DEO-SPD beads exhibited a distinct biphasic kinetic profile characterized by an initial rapid uptake followed by a slower approach to equilibrium (Fig. 7). In the single-solute system, CHI-DEO-SPD beads showed substantial adsorption during the first few hours, with RB4 reaching 132.40 mg/g and Cr(VI) attaining 104.89 mg/g within 4 h. The rapid initial adsorption can be attributed to the abundance of available active sites and the strong concentration gradient between the bulk solution and the bead surface, which enhances external mass transfer [41].

As adsorption progressed, the rate gradually decreased due to the progressive occupation of surface sites, which reduced the driving concentration gradient and introduced intraparticle diffusion resistance. RB4 reached equilibrium earlier than Cr(VI), stabilizing between 8 and 12 h at approximately 189.36 mg/g, whereas Cr(VI) required up to 20 h to reach equilibrium at 159.27 mg/g. The faster equilibration and higher overall uptake of RB4 suggest stronger interactions between the dye molecules and the functionalized CHI-DEO-SPD surface, consistent with multiple binding mechanisms, including electrostatic attraction, hydrogen bonding, and π–π stacking [54]. In the binary-solute system, overall adsorption capacities decreased due to competition for shared active sites. RB4 remained the dominant species, although its equilibrium capacity declined to 151.50 mg/g, while Cr(VI) adsorption decreased more markedly to 95.56 mg/g. Interestingly, equilibrium was reached slightly earlier under binary conditions (12–16 h for both solutes), likely because simultaneous competition accelerated surface saturation and led to earlier steady-state conditions.

To quantitatively describe the adsorption kinetics, the pseudo-first-order (PFO) and pseudo-second-order (PSO) models were applied to the experimental data (Table 3). The PFO model assumes that the adsorption rate is proportional to the number of unoccupied sites and is primarily governed by physical diffusion. In contrast, the PSO model is based on chemisorption involving valence forces through electron sharing or exchange between functional groups on the adsorbent and the adsorbate. For both RB4 and Cr(VI), the PSO model provided a superior fit compared with the PFO model, as indicated by higher correlation coefficients ($R^2 = 0.996–0.999$) and lower chi-square ($\chi^2 = 0.34–2.93$) values. In the single-solute system, RB4 adsorption followed PSO kinetics with $R^2 = 0.999$ and $\chi^2 = 1.28$, while Cr(VI) exhibited similar behavior with $R^2 = 0.999$ and $\chi^2 = 2.93$. The binary-solute system also

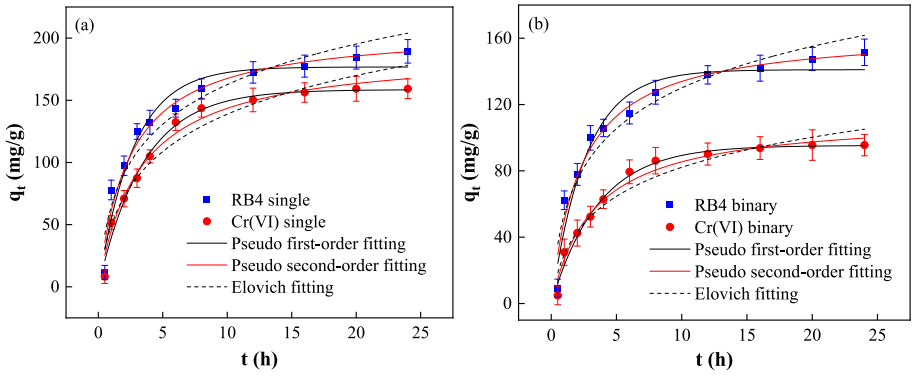

Fig. 7. Adsorption kinetics of RB4 and Cr(VI) onto CHI-DEO-SPD beads in single- and binary-solute systems (1 g/L of beads in 100 mL of 100 mg/L adsorbate solution at pH 3 for 24 h at room temperature).

Table 3
Kinetic model parameters for the adsorption of RB4 and Cr(VI) onto CHI-DEO-SPD beads in single- and binary-solute systems.

Kinetic model	Parameters	Single-solute system		Binary-solute system	
		Cr(VI)	RB4	Cr(VI)	RB4
Experimental data	q_e (mg/g)	159.27	189.36	95.56	151.50
Pseudo-first-order	q_{cal} (mg/g)	155.8	187.2	94.1	149.5
	K_1 (h^{-1})	0.538	0.642	0.685	0.698
	χ^2	3.14	1.83	2.86	0.60
	R^2	0.997	0.998	0.994	0.998
Pseudo-second-order	q_{cal} (mg/g)	160.5	189.5	96.3	151.8
	K_2 (g/(mg·h))	0.0082	0.0091	0.023	0.0125
	χ^2	2.93	1.28	2.24	0.34
	R^2	0.999	0.999	0.996	0.999
Elovich	α (mg/(g·h))	86.86	135.05	53.4	121.22
	β (g/mg)	0.021	0.021	0.037	0.027
	χ^2	3.96	5.32	1.41	3.98
	R^2	0.942	0.924	0.942	0.931

fit the PSO model well (R^2 = 0.996–0.999), confirming that chemisorption is the dominant rate-controlling step for both adsorbates. This indicates the involvement of valence forces through electron sharing or exchange between the adsorbent's amino and hydroxyl groups and the anionic species in solution.

The equilibrium adsorption capacities calculated from the PSO model (q_{cal}) were in excellent agreement with the experimental values (q_e), validating the model's applicability. In the single-solute system, q_{cal} values were 189.5 mg/g for RB4 and 160.5 mg/g for Cr(VI), while in the binary system, they decreased to 151.8 mg/g and 96.3 mg/g, respectively, demonstrating the impact of competitive inhibition on adsorption performance.

The kinetic rate constants further supported these observations. For the PFO model, K_1 values were 0.642 h^{-1} (RB4-single) and 0.538 h^{-1} (Cr(VI)-single), with binary conditions yielding 0.698 h^{-1} (RB4) and 0.685 h^{-1} (Cr(VI)). For the PSO model, K_2 values were 0.0091 g/(mg·h) (RB4-single) and 0.0082 g/(mg·h) (Cr(VI)-single), while binary systems yielded 0.0125 g/(mg·h) (RB4) and 0.023 g/(mg·h) (Cr(VI)). The higher apparent K_2 for Cr(VI) in the binary system, despite its lower equilibrium capacity, suggests a faster initial adsorption process constrained by competition with RB4 molecules for available active sites.

The Elovich model was also employed to interpret the chemisorption process further and assess the surface heterogeneity of CHI-DEO-SPD beads. The Elovich equation assumes that adsorption occurs on energetically heterogeneous surfaces and that the rate decreases exponentially with increasing surface coverage [55]. As shown in Table 3, the Elovich model produced strong linear correlations (R^2 = 0.924–0.942) for all systems, confirming that chemisorption predominates. The initial adsorption rate (α) was higher for RB4 than for Cr(VI) in both single (135.05 vs. 86.86 mg/g·h) and binary (121.22 vs. 53.40 mg/g·h) systems, indicating faster surface interactions for the dye. The β values (0.021–0.037 g/mg) indicate moderate surface heterogeneity, with slightly higher β values in binary systems, likely reflecting competition-induced variations in surface energy distribution. The agreement between the Elovich parameters and PSO results reinforces the conclusion that adsorption proceeds predominantly through heterogeneous chemisorption, involving the interaction of anionic species with protonated amino and hydroxyl groups on the CHI-DEO-SPD surface.

Overall, these findings confirm that the PSO model most accurately describes the adsorption kinetics of both RB4 and Cr(VI) in single- and binary-solute systems. The predominance of PSO kinetics indicates that chemisorption (driven by specific surface interactions and possible coordination between adsorbate ions and protonated amine groups) governs the adsorption mechanism. RB4 exhibits both a stronger affinity and a faster equilibrium rate than Cr(VI), consistent with its multiple binding pathways and larger aromatic structure, which enable π–π stacking, hydrogen bonding, and electrostatic attraction. Cr(VI) adsorption, by contrast, is largely restricted to electrostatic mechanisms. The kinetic analysis thus underscores the importance of evaluating adsorption behavior under competitive multicomponent conditions, which more closely replicate industrial wastewater environments and yield a realistic assessment of adsorbent performance.

3.6. Adsorption isotherms

The Langmuir and Freundlich isotherm models were employed to analyze the equilibrium adsorption behavior of RB4 and Cr(VI) onto CHI-DEO-SPD beads. These models provide critical insights into the adsorption mechanisms, surface heterogeneity, and the nature of adsorbate–adsorbent interactions. The Langmuir model assumes monolayer adsorption onto a homogeneous surface with identical, energetically equivalent sites, while the Freundlich model is an empirical equation describing adsorption on heterogeneous surfaces [56].

The experimental isotherms for both solutes in single- and binary-solute systems are presented in Fig. 8. The adsorption capacity for all systems increased with the initial adsorbate concentration, exhibiting a steep rise at low concentrations that gradually plateaued at higher concentrations. This shape indicates a high affinity between the adsorbates and the CHI-DEO-SPD surface at low concentrations and progressive saturation of available binding sites at higher loadings [57].

The corresponding Langmuir and Freundlich parameters, obtained via nonlinear regression analysis, are summarized in Table 4. Both models fitted the equilibrium data well, with R^2 generally exceeding 0.99; however, the Freundlich model consistently provided a superior fit, as evidenced by lower χ^2 values (Table 4). This outcome suggests that adsorption occurs predominantly on a heterogeneous surface with sites of varying affinity, consistent with the structural characteristics of chitosan-based materials. The glucosamine and *N*-acetylglucosamine units of chitosan furnish both amino and hydroxyl groups, enabling diverse adsorption mechanisms, including electrostatic attraction, hydrogen bonding, and coordination-type interactions [58].

The Freundlich parameters further highlight the differences in adsorption behavior between RB4 and Cr(VI). In single-solute systems, RB4 displayed higher K_F values than Cr(VI) at all temperatures, with values of 7.6, 6.21, and 4.73 $(mg/g)(mg/L)^{1/n}$ at 25, 35, and 45 °C, respectively. The corresponding n values (≈1.44–1.45) indicate favorable adsorption ($n > 1$), reflecting strong binding intensity and high surface heterogeneity [59]. These results align with the structural complexity of RB4, which possesses multiple sulfonate groups and aromatic rings, consistent with adsorption on heterogeneous surfaces and potential multi-mechanistic interactions such as electrostatic attraction, hydrogen bonding, and π–π stacking.

In binary-solute systems, K_F values for RB4 decreased slightly, and Langmuir monolayer capacities (q_m) dropped more sharply, from 872.35 mg/g (single) to 715.26 mg/g (binary) at 25 °C, from 670.61 to 554.46 mg/g at 35 °C, and from 539.82 to 347.51 mg/g at 45 °C. The more pronounced decline at elevated temperatures indicates that RB4 adsorption is exothermic and highly sensitive to competition with Cr(VI). Conversely, in single-solute systems, Cr(VI) exhibited lower K_F values (5.37, 4.62, and 4.15 across 25–45 °C) and slightly smaller n values (1.38 to 1.34), still indicating favorable but less intense adsorption than RB4. Notably, Cr(VI) exhibited increasing q_m values that increased with temperature (739.91, 756.27, and 785.19 mg/g), reflecting an endothermic adsorption process. This behavior implies that higher temperatures enhance Cr(VI) mobility and facilitate diffusion into internal binding sites.

Under binary conditions, Cr(VI) q_m values decreased only modestly (699.92, 724.93, and 760.01 mg/g), and K_F increased slightly with temperature, reaching 5.7 at 45 °C. These results suggest that the competitive inhibition of Cr(VI) adsorption by RB4 weakens at elevated temperatures and that competitive effects diminish as thermal energy

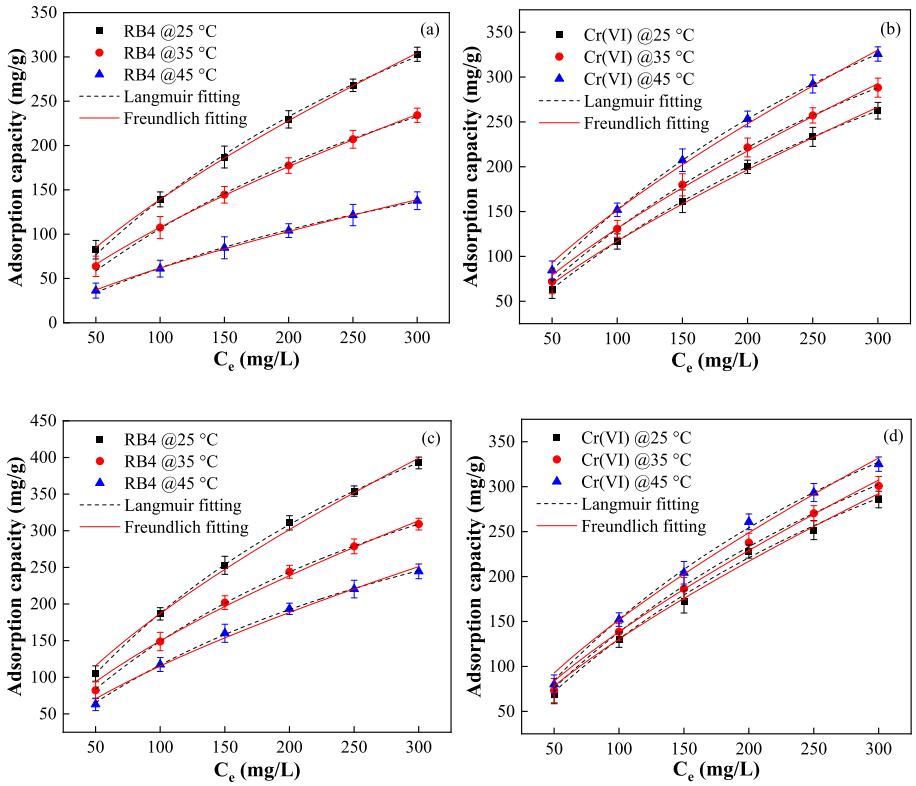

Fig. 8. Adsorption isotherms of RB4 and Cr(VI) onto CHI-DEO-SPD beads in single-solute systems (a, b) and binary-solute systems (c, d) (1 g/L of beads in 100 mL of adsorbate solution at pH 3 for 24 h at 25, 35, and 45 °C).

Table 4
Isotherm parameters for the adsorption of RB4 and Cr(VI) onto CHI-DEO-SPD beads in single- and binary-solute systems.

Adsorbate	Langmuir				Freundlich			
	q_m (mg/g)	K_L (L/mg)	χ^2	R^2	K_F (mg/g)/(mg/L)$^{1/n}$	n	χ^2	R^2
Single-solute								
RB4 @25 °C	872.35	0.0027	67.8	0.995	7.6	1.44	1.75	0.999
RB4 @35 °C	670.61	0.0028	49.8	0.994	6.21	1.45	0.80	0.999
RB4 @45 °C	539.82	0.0027	41.52	0.992	4.73	1.44	2.761	0.999
Cr(VI) @25 °C	739.91	0.0021	87.99	0.991	5.37	1.38	30.07	0.996
Cr(VI) @35 °C	756.27	0.0022	56.89	0.994	4.62	1.36	10.63	0.998
Cr(VI) @45 °C	785.19	0.0023	64.33	0.992	4.15	1.34	19.76	0.998
Binary-solute								
RB4 @25 °C	715.26	0.0024	67.8	0.995	7.59	1.44	14.62	0.998
RB4 @35 °C	554.46	0.0024	49.78	0.994	6.21	1.45	8.71	0.998
RB4 @45 °C	347.51	0.0021	41.52	0.992	4.73	1.43	2.15	0.999
Cr(VI) @25 °C	699.92	0.0020	18.01	0.997	3.65	1.32	4.14	0.998
Cr(VI) @35 °C	724.93	0.0022	24.75	0.997	4.41	1.36	1.69	0.999
Cr(VI) @45 °C	760.01	0.0025	37.39	0.996	5.7	1.40	1.00	0.999

increases, likely due to improved adsorbate diffusion and increased access to deeper sorption sites.

Taken together, these findings indicate that RB4 adsorption follows a heterogeneous and exothermic process strongly influenced by surface heterogeneity and competitive interactions. In contrast, Cr(VI) adsorption, while often conceptualized as a site-specific electrostatic interaction, is best described by the Freundlich model, indicating significant surface energy heterogeneity. The process is endothermic and comparatively resilient under binary conditions. The consistently high q_m values for both adsorbates underscore the excellent performance of CHI-DEO-SPD beads and confirm their versatility for the simultaneous removal of dyes and heavy metals in complex wastewater environments.

The q_m parameter is a critical indicator of an adsorbent's efficiency. Comparing q_m values across studies provide meaningful benchmarks for evaluating relative performance. In this study, the highest q_m for RB4 in single-solute systems was 872.35 mg/g at 25 °C and pH 3, markedly higher than most previously reported adsorbents. For example, guar gum–graft–poly(acrylamide)/silica [60] and peanut shell activated carbon modified with ionic liquid [61] achieved 579.01 mg/g and 364.14 mg/g, respectively. Other chitosan- or carbon-based sorbents typically exhibit capacities below 300 mg/g. These comparisons clearly demonstrate the exceptional affinity of CHI-DEO-SPD beads for dye adsorption.

Similarly, for Cr(VI) in single-solute systems, CHI-DEO-SPD beads achieved a maximum capacity of 785.19 mg/g at 45 °C and pH 3, surpassing most reported materials. For instance, *Parthenium hysterophorus*-based biochar-Fe_3O_4 [62] and polypyrrole-PAN/PEI [63] reached only 400 mg/g and 368 mg/g, respectively, while Fe—Mn oxide-modified

biochar [64] and magnetic kaolin–chitosan beads [65] showed lower capacities (118.03 and 144 mg/g). The superior performance of CHI-DEO-SPD beads can be attributed to the combined effects of structural stabilization and surface functionalization. DEO cross-linking improves the acid stability of chitosan and preserves bead integrity under the acidic conditions required for effective RB4 and Cr(VI) removal. At the same time, SPD functionalization introduces additional protonatable amino groups, increasing the positive surface charge and strengthening electrostatic attraction toward RB4 sulfonate groups and Cr(VI) oxyanions. The increased BET surface area, refined mesoporous structure, and reduced crystallinity further improve the accessibility of active sites and facilitate adsorbate diffusion. For RB4, adsorption is additionally supported by hydrogen bonding and possible dye–dye π-associated interactions, whereas Cr(VI) uptake is mainly governed by electrostatic attraction and interactions with amino and hydroxyl groups. Therefore, the high adsorption capacities of CHI-DEO-SPD beads arise from the combined contribution of abundant active sites, improved pore accessibility, enhanced acid stability, and strong affinity toward anionic pollutants. These results demonstrate the potential of CHI-DEO-SPD beads as a versatile, high-capacity, and reusable adsorbent for industrial wastewater treatment (Table 5).

3.7. Thermodynamic study

Thermodynamic parameters derived from adsorption data are essential for understanding the feasibility, energetic nature, and molecular mechanisms governing adsorption processes. These parameters provide crucial insights into the interactions between adsorbate molecules and adsorbent surfaces, helping to determine whether the process is spontaneous, endothermic, or exothermic, and to assess the degree of molecular organization at the solid–liquid interface [69]. The standard Gibbs free energy (ΔG°), enthalpy (ΔH°), and entropy (ΔS°) changes for the adsorption of RB4 and Cr(VI) onto CHI-DEO-SPD beads were determined from temperature-dependent Langmuir constants using the van't Hoff equation (Table 6). Thermodynamic parameters were evaluated for both single- and binary-solute systems to assess the influence of competitive adsorption on the energetic nature of the process. All calculations were performed within the temperature range of 25–45 °C at pH 3.

The calculated ΔG° values were negative across the studied temperature range for all systems (Table 6), indicating that the adsorption process is thermodynamically spontaneous under the given conditions. For RB4 in the single system, ΔG° ranged from −18.5 to −19.7 kJ/mol, while for Cr(VI) it varied from −13.6 to −14.8 kJ/mol. In the binary system, ΔG° values remained negative and similar in magnitude (−18.2 to −19.0 kJ/mol for RB4; −13.5 to −15.0 kJ/mol for Cr(VI)), confirming that co-adsorption remains spontaneous even under competitive conditions. The magnitude of ΔG° (between −10 and −20 kJ/mol) is characteristic of processes driven by a combination of physical interactions, such as electrostatic attraction and hydrogen bonding, which are reversible and typical for adsorption onto biopolymer-based materials [70].

The ΔH° values revealed distinct and system-dependent energetic behaviors for the two adsorbates (Table 6). In the single-solute system, RB4 adsorption exhibited a slightly negative ΔH° (−1.25 kJ/mol), indicating a weakly exothermic process. This is consistent with the observed decrease in adsorption capacity with increasing temperature (Table 4) and aligns with adsorption mechanisms dominated by electrostatic and π–π interactions, which are often slightly weakened at higher temperatures [71]. However, in the binary system, RB4 adsorption became endothermic (ΔH° = +9.23 kJ/mol). This marked shift suggests that the presence of competing Cr(VI) oxyanions imposes an energetic penalty on RB4 uptake, likely due to restricted access to high-affinity sites and the need for molecular reorientation on a partially occupied surface.

For Cr(VI) in the single-solute system, adsorption exhibited a small positive ΔH° (+1.52 kJ/mol), confirming an endothermic process [72]. The positive enthalpy suggests that adsorption requires a modest energy input, likely associated with the dehydration of Cr(VI) oxyanions and their diffusion to the adsorbent surface. Under binary conditions, the endothermic nature of Cr(VI) adsorption became substantially more pronounced (ΔH° = +15.30 kJ/mol), indicating that its uptake becomes strongly dependent on thermal activation when RB4 occupies a significant portion of the available cationic sites. The endothermic character in both systems explains the increase in Cr(VI) uptake with temperature, as thermal energy enhances ion mobility and may promote stronger surface complexation.

The ΔS° values were positive for both adsorbates in all systems, indicating an increase in randomness at the solid–liquid interface during adsorption. In single systems, ΔS° values were +0.058 kJ/(mol·K) for RB4 and +0.051 kJ/(mol·K) for Cr(VI). These values increased notably in binary systems, reaching +0.092 kJ/(mol·K) for RB4 and +0.097 kJ/(mol·K) for Cr(VI). A positive entropy change often reflects the displacement of ordered water molecules from the hydration shells of the adsorbates or from the adsorbent surface, leading to a net increase in system disorder. The higher ΔS° values observed under competitive conditions suggest greater interfacial disorder, consistent with the simultaneous adsorption of two dissimilar anionic species and the displacement of additional water molecules.

Overall, the thermodynamic analysis demonstrates that the adsorption of both RB4 and Cr(VI) onto CHI-DEO-SPD beads is spontaneous ($\Delta G^\circ < 0$) and accompanied by an increase in entropy ($\Delta S^\circ > 0$). RB4

Table 5
Comparison of maximum adsorption capacities (q_m) of various adsorbents for RB4 and Cr(VI).

Adsorbent	pH	q_m (mg/g)	Ref.
RB4			
Chitosan-hydroxyapatite nanocomposite	4	166.8	[66]
Activated carbon from *Enteromorpha prolifera*	6	131.93	[50]
Poly (methylmethacrylate) grafted chitosan	4	204	[67]
Peanut shell modified by ionic liquid	2	290	[61]
Peanut shell activated carbon modified by ionic liquid	2	364.14	[61]
Guar gum-graft-*poly* (acrylamide)/silica	2	579.01	[60]
CHI-DEO-SPD beads	3	872.35	Present study
Cr(VI)			
$CaFe_2O_4$@rGO-modified biochar	2	30.8	[68]
Fe-Mn oxide-modified biochar	2	118.03	[64]
Parthenium hysterophorus-based biochar-Fe_3O_4	3	400	[62]
Polypyrrole-PAN/PEI	2	368	[63]
Magnetic kaolin-embedded chitosan beads	2	144	[65]
CHI-DEO-SPD beads	3	785.19	Present study

Table 6
Thermodynamic parameters for the adsorption of RB4 and Cr(VI) onto CHI-DEO-SPD beads in single- and binary-solute systems (pH 3, 25–45 °C).

System	Adsorbate	T (K)	ΔG° (kJ/mol)	ΔH° (kJ/mol)	ΔS° (kJ/mol·K)
Single	RB4	298.15	−18.5	−1.25	0.058
		308.15	−19.2		
		318.15	−19.7		
	C(VI)	298.15	−13.6	1.52	0.051
		308.15	−14.2		
		318.15	−14.8		
Binary	RB4	298.15	−18.2	9.23	0.092
		308.15	−18.8		
		318.15	−19.0		
	C(VI)	298.15	−13.5	15.30	0.097
		308.15	−14.2		
		318.15	−15.0		

adsorption transitions from weakly exothermic in single systems to endothermic under competition, while Cr(VI) adsorption remains endothermic but becomes substantially more energy-intensive in binary systems. These results underline the role of distinct yet complementary mechanisms and reveal that competitive interactions not only reduce equilibrium capacities but also fundamentally alter the thermodynamic driving forces of adsorption. The favorable thermodynamics, together with the high capacities observed in both single and binary systems, confirm that CHI-DEO-SPD beads provide an energetically stable and efficient platform for the simultaneous removal of anionic dyes and heavy-metal ions from acidic wastewater.

3.8. Adsorption mechanism

Fig. 9 illustrates the proposed mechanisms governing the adsorption of RB4 and Cr(VI) onto CHI-DEO-SPD beads. The exceptionally high adsorption efficiency of the beads arises from the abundance of surface functional groups (particularly $-NH_2$ and $-OH$ groups), which play pivotal roles in both physical and chemical adsorption. In the case of RB4 adsorption, the amino groups on CHI-DEO-SPD are protonated under acidic conditions to form $-NH_3^+$ species. These cationic sites interact strongly with the anionic sulfonate groups ($-SO_3^-$) of RB4 molecules via electrostatic attraction [73]. This Coulombic interaction serves as the primary driving force for the initial attachment of RB4 onto the adsorbent surface. Beyond electrostatic forces, hydrogen bonding significantly enhances the stability of the adsorbed layer. The hydroxyl and amino groups of CHI-DEO-SPD can form hydrogen bonds with oxygen or nitrogen atoms in the sulfonate and aromatic structures of RB4, further stabilizing the adsorbate–adsorbent complex [74]. Additionally, potential π–π stacking or n–π interactions between the aromatic rings of RB4 and electron-rich regions (e.g., glycosidic oxygen atoms) on the polysaccharide chain contribute to further stabilization [75]. These combined interactions account for the high affinity of CHI-DEO-SPD beads for RB4, as observed in both single- and binary-solute systems.

Spectroscopic and structural evidence corroborates these mechanistic interpretations. FTIR analysis revealed a noticeable shift in the amide I band from 1661 to 1635 cm^{-1}, along with a decrease in the intensity of the N—H bending band (1590–1560 cm^{-1}), broadening of the O–H/N–H stretching region (3300–3500 cm^{-1}), and the emergence of new sulfonate-related peaks at 1200 and 1045 cm^{-1} (Fig. 3a). These spectral modifications confirm the participation of amino and hydroxyl groups in electrostatic and hydrogen-bonding interactions with RB4. Complementary XRD results showed reduced crystallinity, peak broadening, and slight shifts toward lower diffraction angles (Fig. 4a), suggesting partial disruption of the chitosan polymeric structure due to the adsorption and potential intercalation of large RB4 molecules within the matrix.

Morphological analysis further supports these findings. SEM images of pristine CHI-DEO-SPD beads revealed a rough, irregular, and porous surface. Following adsorption, the bead surfaces became smoother and more compact, indicative of pore blockage and the formation of a surface layer. This morphological transformation was more pronounced for RB4 than for Cr(VI), as the bulky aromatic RB4 molecules interact more extensively with the polymeric network (Fig. 5c).

In contrast, Cr(VI) adsorption occurs through a combination of physisorption and chemisorption mechanisms. Under acidic conditions, the protonated amino groups ($-NH_3^+$) on CHI-DEO-SPD act as positively charged active sites that electrostatically attract anionic Cr(VI) species such as CrO_4^{2-} and $HCrO_4^-$. This electrostatic interaction is strongest at low pH, when the surface is highly protonated. However, adsorption is not governed by electrostatic forces alone; surface complexation also plays a significant role. The reactive $-NH_2$ and $-OH$ groups can coordinate with Cr(VI) species, forming both outer-sphere (electrostatic) and inner-sphere (ligand-exchange) complexes, depending on local pH and redox conditions.

At pH ≈ 3, where $HCrO_4^-$ predominates, Cr(VI) is likely to form inner-sphere complexes through ligand exchange between oxygen atoms in the oxyanion and surface hydroxyl or amino groups. FTIR spectra confirmed these interactions by showing changes in N—H stretching vibrations, along with new Cr—O stretching bands at approximately 940 and 885 cm^{-1}, and a less intense band at 780 cm^{-1} associated with dichromate species. Broadening of the O–H/N–H stretching region further supports the involvement of surface functional groups in coordination-type bonding. XRD analysis also corroborated these findings, displaying decreased peak intensities and broadened diffraction patterns after Cr(VI) adsorption (Fig. 4a), indicative of partial structural

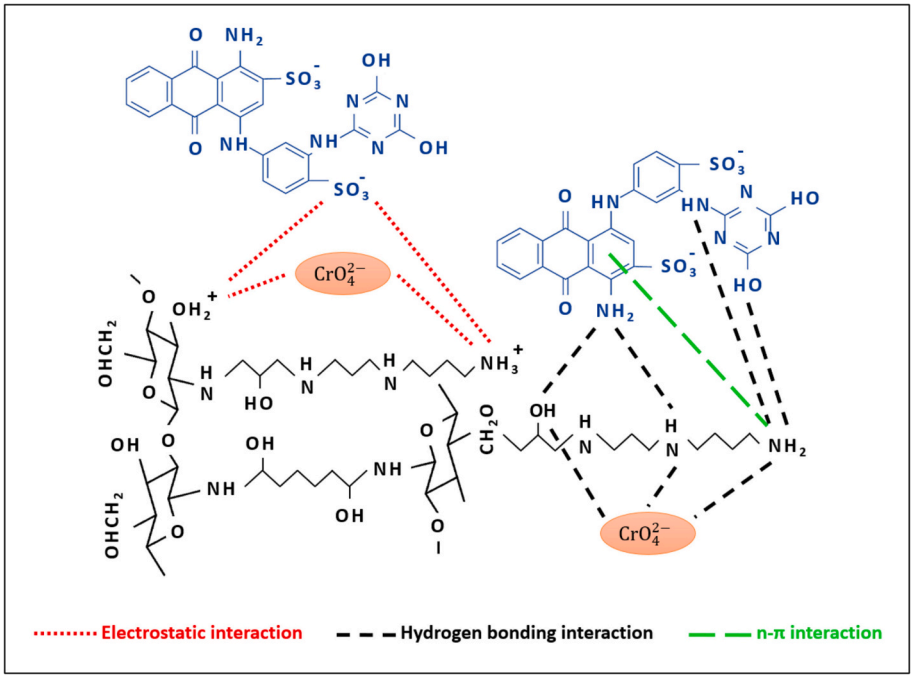

Fig. 9. Proposed mechanisms of RB4 and Cr(VI) adsorption on CHI-DEO-SPD beads.

rearrangement and reduced crystallinity. Unlike RB4, Cr(VI) ions adsorb primarily on external surfaces or near-surface pores through electrostatic attraction and coordination bonding. Intraparticle diffusion facilitates the transport of Cr(VI) species into internal pores, while weak van der Waals forces may also contribute [76].

In the binary-solute system, containing both RB4 and Cr(VI), competition for active sites alters both the adsorption pathway and the relative affinity of each species. Although both adsorbates interact with the same surface functional groups ($-NH_3^+$ and $-OH$), the strength and complexity of their interactions differ markedly. RB4, with its large aromatic framework and multiple sulfonate groups, can engage in multiple simultaneous interactions (electrostatic attraction, hydrogen bonding, and possible π–π interactions), thereby occupying active sites more effectively. Cr(VI), on the other hand, relies predominantly on electrostatic attraction and surface complexation. In the presence of RB4, many surface-NH_3^+ sites become occupied by dye molecules, reducing the number of accessible cationic sites for Cr(VI) binding.

Nevertheless, Cr(VI) adsorption still proceeds via coordination with residual –OH and unprotonated $–NH_2$ groups and through diffusion into unoccupied inner pores. Interestingly, the coexistence of both adsorbates generates competitive yet partially synergistic effects. While RB4 adsorption can physically block pores, it also increases the local positive charge density, which may enhance the electrostatic attraction of Cr(VI) species to adjacent binding sites. This phenomenon may account for the observed moderation in the competitive suppression of Cr(VI) uptake at higher temperatures under binary conditions.

The experimentally observed competitive adsorption behavior is consistent with the thermodynamic and isotherm analyses. RB4 adsorption is exothermic and site-specific, whereas Cr(VI) adsorption is endothermic and involves significant diffusive transport. Consequently, in multicomponent systems, RB4 preferentially occupies high-affinity surface sites, while Cr(VI) adsorbs onto lower-energy or diffusion-accessible sites through thermally activated mechanisms.

In summary, the adsorption of RB4 onto CHI-DEO-SPD is governed by a combination of electrostatic attraction, hydrogen bonding, and π–π interactions, resulting in strong binding and measurable structural modification of the adsorbent, as verified by FTIR, XRD, and SEM analyses. In contrast, Cr(VI) adsorption primarily involves electrostatic attraction and surface complexation, with diffusion processes contributing to the uptake. In binary-solute systems, competitive adsorption introduces additional complexity: RB4 dominates due to its multifunctional binding capabilities, while Cr(VI) uptake is modulated by residual site availability and thermal activation. The interplay among electrostatic, hydrogen-bonding, and coordination mechanisms enables CHI-DEO-SPD beads to efficiently capture both large organic dyes and inorganic oxyanions, confirming their versatility, robustness, and potential as an advanced adsorbent for industrial wastewater treatment applications. It is important to acknowledge that while the adsorption mechanism has been comprehensively investigated through experimental techniques including FTIR, XRD, SEM, zeta potential, and kinetic/isotherm modeling, theoretical validation using Density Functional Theory (DFT) simulations was beyond the scope of the present study. DFT calculations would provide valuable atomic-level insights into adsorption configurations, binding energies, and charge transfer processes between RB4/Cr(VI) and the functional groups of CHI-DEO-SPD beads. Such theoretical analysis would complement the experimental findings presented here and could guide future structural optimization of the adsorbent. Therefore, DFT simulations are recommended as an important direction for subsequent investigations.

3.9. Adsorbent reusability

The recovery and reusability of adsorbents are critical parameters for evaluating their economic and practical feasibility in real-world wastewater treatment systems. Efficient regeneration directly influences material sustainability, operational cost, and environmental compatibility. The surface charge of CHI-DEO-SPD beads (highly sensitive to pH) plays a decisive role in determining regeneration behavior after desorption.

In most adsorption systems, alkaline solutions are commonly employed for desorption and regeneration because hydroxide ions effectively compete with anionic contaminants for active sites. Hydroxide ions displace bound species such as RB4 and Cr(VI) from protonated amino and hydroxyl groups, weakening electrostatic interactions and promoting contaminant release. Accordingly, a 1.0 mol/L NaOH solution was used in this study for regenerating CHI-DEO-SPD beads [77]. The observed decrease in adsorption efficiency under alkaline conditions (Fig. 6c) supports this approach: high pH values neutralize the surface charge by converting protonated $-NH_3^+$ groups back to their neutral $–NH_2$ form, thereby diminishing electrostatic attraction toward negatively charged RB4 ($-SO_3^-$) and Cr(VI) species ($HCrO_4^-$, $Cr_2O_7^{2-}$). This pH-dependent mechanism underlies the desorption and regeneration strategy adopted here.

Desorption and regeneration experiments demonstrated that CHI-DEO-SPD beads could be reused effectively for multiple adsorption–desorption cycles. However, a gradual decline in adsorption capacity was observed with repeated use (Fig. 10). For RB4, the initial adsorption capacity was 200.71 mg/g in the first cycle, decreasing slightly to 195.86 mg/g by the third cycle (a 2.4% reduction). By the fifth cycle, the capacity dropped to 180.39 mg/g (a 10.1% reduction). A more significant decline was observed in later cycles, with RB4 adsorption capacity falling to 82.46 mg/g after the tenth cycle (a 58.9% reduction) and to 19.59 mg/g after the fifteenth cycle (a 90.2% reduction).

The gradual loss of adsorption capacity with successive regeneration cycles can be attributed to several interrelated mechanisms. Repeated exposure to strong alkaline desorption media progressively deprotonates surface amino groups, reducing the number of positively charged $–NH_3^+$ sites available for electrostatic interaction with RB4's sulfonate ($–SO_3^-$) groups. Additionally, repeated swelling and contraction during adsorption and desorption induce mechanical fatigue, leading to partial pore collapse and diminished surface accessibility. Secondary forces, such as hydrogen bonding and n–π interactions, also weaken over time due to molecular rearrangements and structural relaxation. Moreover, incomplete desorption of strongly bound RB4 molecules leads to progressive site blocking, further limiting active-site availability in subsequent cycles [77].

A similar but more pronounced decline was observed for Cr(VI). The initial adsorption capacity of 139.49 mg/g decreased moderately to 131.50 mg/g by the third cycle (a 5.7% reduction) and to 115.68 mg/g

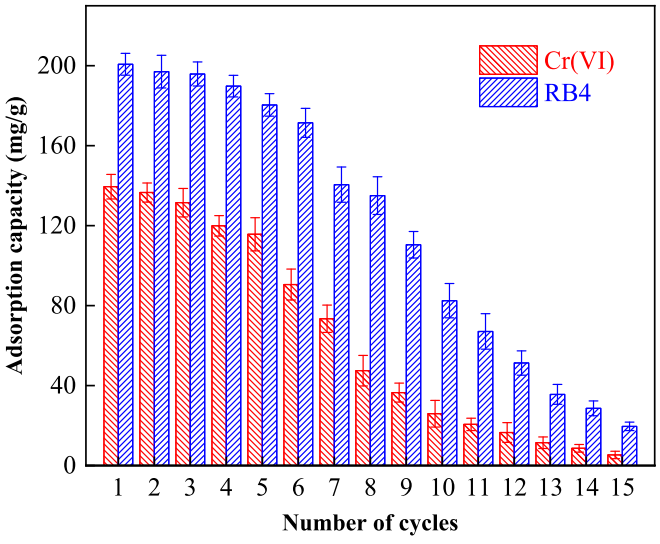

Fig. 10. Effect of regeneration cycles on the RB4 and Cr(VI) adsorption capacity of the CHI-DEO-SPD beads.

by the fifth cycle (a 17% reduction). The decline accelerated rapidly thereafter, with Cr(VI) adsorption capacity dropping to 25.94 mg/g after the tenth cycle (an 81.4% reduction) and to 5.31 mg/g after the fifteenth cycle (a 96% reduction).

This steep decline is primarily due to the oxidative nature of Cr(VI). Chromate (CrO_4^{2-}) and dichromate ($Cr_2O_7^{2-}$) ions are strong oxidizing agents capable of reacting with chitosan's amino and hydroxyl groups, leading to the chemical degradation of active sites and progressive weakening of the polymer matrix [78]. Repeated alkaline regeneration also contributes to deacetylation, chain scission, and partial depolymerization of chitosan, thereby reducing mechanical integrity and adsorption capacity.

Additionally, incomplete desorption of residual chromium species (particularly those involved in inner-sphere complexation) leads to cumulative surface fouling. Consequently, both the number of reactive sites and the available pore volume decrease with successive cycles. Notably, the primary degradation mechanisms differ between the two adsorbates. For RB4, performance loss is mainly due to physical and mechanical factors: site saturation, pore blockage, and fatigue from swelling/contraction. For Cr(VI), the decline stems more from chemical degradation: oxidative damage to the polymer backbone and functional groups, which is more rapid and irreversible. This distinction is consistent with the observation that Cr(VI)-loaded beads exhibited visible discoloration and increased brittleness after several cycles, whereas RB4-loaded beads retained better structural cohesion over the same period.

Overall, these findings indicate that CHI-DEO-SPD beads exhibit strong short-term regenerability but limited long-term stability. For both RB4 and Cr(VI), adsorption capacity remained above 50% of the initial value for the first 8–10 regeneration cycles. Beyond this point, the decline became more pronounced, with efficiencies dropping below levels typically acceptable for industrial-scale wastewater treatment. These results align with previous observations for chitosan-based adsorbents, where long-term degradation is often attributed to oxidative attack, alkaline hydrolysis, and cumulative site occupation [77,78]. While the 15-cycle test provides valuable insight into durability, it also underscores the limitations of repeated NaOH-based regeneration. For large-scale applications, alternative regeneration strategies, such as milder alkaline agents, chelating solutions, or electrochemical desorption, could extend the operational lifetime of CHI-DEO-SPD beads while minimizing structural degradation. Therefore, under the conditions tested, CHI-DEO-SPD beads can be effectively reused for approximately 8–10 adsorption–desorption cycles, maintaining high removal efficiency and mechanical stability before requiring replacement or chemical reinforcement.

4. Conclusions

This study developed CHI-DEO-SPD beads as a high-performance biopolymeric adsorbent for the removal of Cr(VI) and RB4 from acidic aqueous systems. The dual-modification strategy combined the structural reinforcement provided by DEO cross-linking with the increased amine density introduced by SPD functionalization, thereby addressing two major limitations of conventional chitosan adsorbents: poor acid stability and limited adsorption capacity. Comprehensive characterization confirmed successful chemical modification, reduced crystallinity, improved thermal stability, refined mesoporosity, and a substantial increase in surface area from 4.59 to 34.60 m^2/g. The pHpzc value of 6.3 indicated that the beads remain positively charged under acidic conditions, favoring the electrostatic attraction of anionic Cr(VI) species and sulfonated RB4 molecules.

Under optimized synthesis conditions of 1.5 g/L SPD, 40 °C, and 3 h reaction time, CHI-DEO-SPD beads exhibited excellent adsorption performance. In single-solute systems, the maximum Langmuir adsorption capacities reached 872.35 mg/g for RB4 and 785.19 mg/g for Cr(VI). In the binary system, the capacities remained high at 715.26 mg/g for RB4 and 699.92 mg/g for Cr(VI), although the decrease relative to single-solute systems confirmed competitive adsorption between coexisting anionic pollutants. Kinetic data were best described by the pseudo-second-order model, suggesting that chemisorption played a major role in the adsorption process. The Freundlich model provided the best fit for equilibrium data, indicating heterogeneous multilayer adsorption involving electrostatic interactions, hydrogen bonding, and, particularly for RB4, possible π–π interactions. Thermodynamic analysis showed that adsorption was spontaneous in all systems, while differences in enthalpy behavior revealed that competitive adsorption altered the energetic requirements of pollutant uptake.

The broader significance of this work lies in its contribution to the design of sustainable, multifunctional adsorbents for complex wastewater treatment. Many adsorbents perform well in single-contaminant systems but lose efficiency when exposed to mixed pollutants. In contrast, CHI-DEO-SPD beads maintained high adsorption capacities under binary Cr(VI)/RB4 conditions, which more closely resemble effluents from textile dyeing, chrome plating, and related industrial processes. The use of chitosan as a renewable polymer, combined with amine-rich functionalization and acid-resistant cross-linking, provides a promising platform for developing practical adsorbents capable of treating wastewater streams containing both heavy metals and synthetic dyes. The regeneration results further support the practical relevance of the material, as the beads retained substantial adsorption capacity over repeated adsorption–desorption cycles.

Despite these promising findings, several limitations should be acknowledged. First, the adsorption experiments were conducted using synthetic aqueous solutions under controlled laboratory conditions. Therefore, the influence of real wastewater constituents, including competing ions, dissolved organic matter, salts, surfactants, suspended solids, and fluctuating pH, remains to be fully evaluated. Second, the study focused on batch adsorption, and continuous-flow column experiments are needed to determine breakthrough behavior, hydraulic performance, mass-transfer limitations, and long-term operational stability. Third, although the RB4/Cr(VI) binary system provides a more realistic assessment than single-solute experiments, actual industrial wastewater contains more complex mixtures of dyes, metals, salts, and auxiliary chemicals that may affect adsorption selectivity and capacity. Fourth, while NaOH regeneration was effective, repeated alkaline treatment caused gradual performance decline, indicating the need to explore milder, less destructive regeneration approaches. Finally, scale-up factors, including synthesis cost, adsorbent leaching, mechanical durability, disposal or recovery of spent beads, and techno-economic feasibility, were not addressed in this work.

Overall, CHI-DEO-SPD beads demonstrate strong potential as a sustainable, reusable, and acid-stable adsorbent for treating wastewater containing coexisting anionic dyes and Cr(VI). By maintaining high adsorption performance under binary conditions, this material offers a promising platform for addressing complex industrial effluents where dyes and heavy metals occur simultaneously. Future work should focus on validation with real wastewater, continuous-flow operation, optimized regeneration, and techno-economic assessment to support practical implementation.

CRediT authorship contribution statement

Mohammadtaghi Vakili: Writing – review & editing, Writing – original draft, Visualization, Validation, Supervision, Software, Methodology, Investigation, Formal analysis, Data curation. **Zahra Gholami:** Writing – review & editing, Visualization, Formal analysis. **Babak Salamatinia:** Writing – review & editing, Methodology, Data curation.

Declaration of competing interest

The authors declare that they have no known competing financial interests or personal relationships that could have appeared to influence

the work reported in this paper.

Acknowledgment

The publication was supported by the project RUR - Region for university, university for region, reg. no. CZ.10.02.01/00/22_002/0000210, co-financed by the European Union. The publication was created at the Department of Chemistry of the Faculty of Science, J. E. Purkyně University in Ústí nad Labem, Czech Republic.

Data availability

The data that has been used is confidential.

References

[1] I. Salahshoori, Q. Wang, M.A.L. Nobre, A.H. Mohammadi, E.A. Dawi, H. A. Khonakdar, Molecular simulation-based insights into dye pollutant adsorption: a perspective review, Adv. Colloid Interf. Sci. 333 (2024) 103281, https://doi.org/10.1016/j.cis.2024.103281.
[2] F. Zaoui, B. Elhadj-Daouadji, C. Alaoui, N.i. Saleh, C.E. Gherdaoui, M. Beldjilali, T. Chipiri, F. Ibrahim, F.Z. Sebba, B. Bounaceur, H. Ma, Adsorption behaviour of cationic and anionic dyes on new chitosan-activated carbon@metal oxide hydrogels beads: effect of the metal nature and comparative study, Int. J. Biol. Macromol. 312 (2025) 144186, https://doi.org/10.1016/j.ijbiomac.2025.144186.
[3] L. Boughrara, F.Z. Sebba, H. Sebti, E. Choukchou-Braham, B. Bounaceur, S.O. Kada, F. Zaoui, Removal of Zn(II) and Ni(II) heavy metal ions by new alginic acid-ester derivatives materials, Carbohydr. Polym. 272 (2021) 118439, https://doi.org/10.1016/j.carbpol.2021.118439.
[4] P. Sharma, S.P. Singh, S.K. Parakh, Y.W. Tong, Health hazards of hexavalent chromium (Cr (VI)) and its microbial reduction, Bioengineered 13 (2022) 4923–4938, https://doi.org/10.1080/21655979.2022.2037273.
[5] N.S. Hassan, A.A. Jalil, M.B. Bahari, N.M. Izzuddin, N.A.F.M. Fauzi, N.W.C. Jusoh, M.F.A. Kamaroddin, R. Saravanan, H. Tehubijuluw, A critical review of MXene-based composites in the adsorptive and photocatalysis of hexavalent chromium removal from industrial wastewater, Environ. Res. 259 (2024) 119584, https://doi.org/10.1016/j.envres.2024.119584.
[6] S.N. Kamati, J. Yan, J. Fan, A review on progresses in reactive dye-containing wastewater treatment, Water Pract. Technol. 19 (2024) 2712–2733, https://doi.org/10.2166/wpt.2024.142.
[7] L. Hevira, J.O. Ighalo, D. Sondari, Chitosan-based polysaccharides for effective synthetic dye adsorption, J. Mol. Liq. 393 (2024) 123604, https://doi.org/10.1016/j.molliq.2023.123604.
[8] M. Bagchi, L. Ray, Adsorption behavior of Reactive Blue 4, a tri-azine dye on dry cells of Rhizopus oryzae in a batch system, Chem. Speciat. Bioavailab. 27 (2015) 112–120, https://doi.org/10.1080/09542299.2015.1088802.
[9] M.T. Moustafa, Preparation and characterization of low-cost adsorbents for the efficient removal of malachite green using response surface modeling and reusability studies, Sci. Rep. 13 (2023) 4493, https://doi.org/10.1038/s41598-023-31391-4.
[10] M.A. Zorgani, F. Zaoui, R.N.E.H. Zorgani, B. Elhadj Daouadji, F.Z. Sebba, E. Choukchou-Braham, B. Bounaceur, Y. Ma, M. Bhardwaj, H. Ma, Ultrasonic-assisted adsorption of heavy copper and lead metal ions by g-C3N4, application of g-C3N4@MNPs (M: Pb, Cu) in the catalytic photoreduction of organic pollutants, J. Water Process Eng. 58 (2024) 104724, https://doi.org/10.1016/j.jwpe.2023.104724.
[11] B. Elhadj-Daouadji, F. Zaoui, M.A. Zorgani, S. Abubakar, L.A. Siddig, A. S. Abdelhamid, M. Bhardwaj, M. Hachemaoui, M.h. Guezzoul, A. Kumar, B. Bounaceur, F. Lebsir, N.i. Saleh, Efficient removal of asphaltene and organic dyes using hybrid magnetic nanomaterials: adsorption selectivity and comparative study, Fuel 381 (2025) 133284, https://doi.org/10.1016/j.fuel.2024.133284.
[12] S. Afroze, T.K. Sen, A review on heavy metal ions and dye adsorption from water by agricultural solid waste adsorbents, Water Air Soil Pollut. 229 (2018) 1–50, https://doi.org/10.1007/s11270-018-3869-.
[13] J. Pérez-Calderón, M.V. Santos, N. Zaritzky, Synthesis, characterization and application of cross-linked chitosan/oxalic acid hydrogels to improve azo dye (Reactive Red 195) adsorption, React. Funct. Polym. 155 (2020) 104699, https://doi.org/10.1016/j.reactfunctpolym.2020.104699.
[14] A. Fenti, S. Chianese, P. Iovino, D. Musmarra, S. Salvestrini, Cr(VI) sorption from aqueous solution: a review, Appl. Sci. 10 (2020) 6477, https://doi.org/10.3390/app10186477.
[15] M. Vakili, S. Deng, D. Liu, T. Li, G. Yu, Preparation of aminated cross-linked chitosan beads for efficient adsorption of hexavalent chromium, Int. J. Biol. Macromol. 139 (2019) 352–360, https://doi.org/10.1016/j.ijbiomac.2019.07.207.
[16] L. Tsiantouka, P. Haskis, C. Lykos, P. Mpeza, G. Patakioutas, I. Konstantinou, M. Barczak, I. Pashalidis, I. Anastopoulos, Biosorption of Reactive Red 120 dye by Pyracantha coccinea berries powdered biomass, Sustain. Chem. Environ. 7 (2024) 100135, https://doi.org/10.1016/j.scenv.2024.100135.
[17] G.Z. Kyzas, N.K. Lazaridis, M. Kostoglou, On the simultaneous adsorption of a reactive dye and hexavalent chromium from aqueous solutions onto grafted chitosan, J. Colloid Interface Sci. 407 (2013) 432–441, https://doi.org/10.1016/j.jcis.2013.05.052.
[18] A.H. Jawad, S.S.A. Norrahma, B.H. Hameed, K. Ismail, Chitosan-glyoxal film as a superior adsorbent for two structurally different reactive and acid dyes: adsorption and mechanism study, Int. J. Biol. Macromol. 135 (2019) 569–581, https://doi.org/10.1016/j.ijbiomac.2019.05.127.
[19] F. Hong, P. Qiu, Y. Wang, P. Ren, J. Liu, J. Zhao, D. Gou, Chitosan-based hydrogels: from preparation to applications, a review, Food Chem. X. 21 (2024) 101095, https://doi.org/10.1016/j.fochx.2023.101095.
[20] P. Mohammadzadeh Pakdel, S.J. Peighambardoust, Review on recent progress in chitosan-based hydrogels for wastewater treatment application, Carbohydr. Polym. 201 (2018) 264–279, https://doi.org/10.1016/j.carbpol.2018.08.070.
[21] N.H.N. Do, Q.T. Truong, P.K. Le, A.C. Ha, Recent developments in chitosan hydrogels carrying natural bioactive compounds, Carbohydr. Polym. 294 (2022) 119726, https://doi.org/10.1016/j.carbpol.2022.119726.
[22] M. Vakili, S. Deng, T. Li, W. Wang, W. Wang, G. Yu, Novel crosslinked chitosan for enhanced adsorption of hexavalent chromium in acidic solution, Chem. Eng. J. 347 (2018) 782–790, https://doi.org/10.1016/j.cej.2018.04.181.
[23] A. Apirakaramwong, S. Sunthornphan, N. Pasuthawong, T. Intaravicha, N. Ruangthai, T. Rojanarata, P. Opanasopit, The effect of spermidine and spermine on chitosan-mediated gene delivery, Key Eng. Mater. 859 (2020) 113–119, https://doi.org/10.4028/www.scientific.net/KEM.859.113.
[24] M. Vakili, M. Rafatullah, M.H. Ibrahim, A.Z. Abdullah, B. Salamatinia, Z. Gholami, Chitosan hydrogel beads impregnated with hexadecylamine for improved reactive blue 4 adsorption, Carbohydr. Polym. 137 (2016) 139–146, https://doi.org/10.1016/j.carbpol.2015.09.017.
[25] M. Vakili, M. Rafatullah, B. Salamatinia, M.H. Ibrahim, A.Z. Abdullah, Elimination of reactive blue 4 from aqueous solutions using 3-aminopropyl triethoxysilane modified chitosan beads, Carbohydr. Polym. 132 (2015) 89–96, https://doi.org/10.1016/j.carbpol.2015.05.080.
[26] J. Lu, J.S. Brown, C.L. Liotta, C.A. Eckert, Polarity and hydrogen-bonding of ambient to near-critical water: Kamlet–Taft solvent parameters, Chem. Commun. (7) (2001) 665–666, https://doi.org/10.1039/B100425P.
[27] E. Savitri, S.R. Juliastuti, A. Handaratri, Sumarno, A. Roesyadi, Degradation of chitosan by sonication in very-low-concentration acetic acid, Polym. Degrad. Stab. 110 (2014) 344–352, https://doi.org/10.1016/j.polymdegradstab.2014.09.010.
[28] M.K.A. Khan, A.S. Abdulhameed, H. Alshahrani, S. Algburi, Development of chitosan biopolymer by chemically modified orange peel for safranin O dye removal: a sustainable adsorbent and adsorption modeling using RSM-BBD, Int. J. Biol. Macromol. 261 (2024) 129964, https://doi.org/10.1016/j.ijbiomac.2024.129964.
[29] Y. Tamer, A. Koşucu, H. Berber, Graphene oxide incorporated chitosan/acrylamide/itaconic acid semi-interpenetrating network hydrogel bio-adsorbents for highly efficient and selective removal of cationic dyes, Int. J. Biol. Macromol. 219 (2022) 273–289, https://doi.org/10.1016/j.ijbiomac.2022.07.238.
[30] Q. Yuan, J. Shah, S. Hein, R.D.K. Misra, Controlled and extended drug release behavior of chitosan-based nanoparticle carrier, Acta Biomater. 6 (2010) 1140–1148, https://doi.org/10.1016/j.actbio.2009.08.027.
[31] J. Cui, X. Wang, S. Yu, C. Zhong, N. Wang, J. Meng, Facile fabrication of chitosan-based adsorbents for effective removal of cationic and anionic dyes from aqueous solutions, Int. J. Biol. Macromol. 165 (2020) 2805–2812, https://doi.org/10.1016/j.ijbiomac.2020.10.161.
[32] M. Vakili, F. Gholami, H.M. Zwain, W. Wang, A. Mojiri, M. Tomas, G. Cagnetta, R. Gholizadeh, W. Dastyar, Z. Gholami, Removal of GenX by APTES functionalized diepoxyoctane cross-linked chitosan beads, J. Environ. Chem. Eng. 11 (2023) 110539, https://doi.org/10.1016/j.jece.2023.110539.
[33] M. Fathy, H. Selim, A.E. Shahawy, Chitosan/MCM-48 nanocomposite as a potential adsorbent for removing phenol from aqueous solution, RSC Adv. 10 (2020) 23417–23430, https://doi.org/10.1039/D0RA02960B.
[34] H. Ge, S. Wang, Thermal preparation of chitosan–acrylic acid superabsorbent: optimization, characteristic and water absorbency, Carbohydr. Polym. 113 (2014) 296–303, https://doi.org/10.1016/j.carbpol.2014.06.078.
[35] O. Molatlhegi, L. Alagha, Adsorption characteristics of chitosan grafted copolymer on kaolin, Appl. Clay Sci. 150 (2017) 342–353, https://doi.org/10.1016/j.clay.2017.09.032.
[36] M. Jaworska, K. Sakurai, P. Gaudon, E. Guibal, Influence of chitosan characteristics on polymer properties. I: crystallographic properties, Polym. Int. 52 (2003) 198–205, https://doi.org/10.1002/pi.1159.
[37] P. Karthikeyan, S. Meenakshi, Fabrication of hybrid chitosan encapsulated magnetic-kaolin beads for adsorption of phosphate and nitrate ions from aqueous solutions, Int. J. Biol. Macromol. 168 (2021) 750–759, https://doi.org/10.1016/j.ijbiomac.2020.11.132.
[38] M.A. Gámiz-González, D.M. Correia, S. Lanceros-Mendez, V. Sencadas, J.L. Gómez Ribelles, A. Vidaurre, Kinetic study of thermal degradation of chitosan as a function of deacetylation degree, Carbohydr. Polym. 167 (2017) 52–58, https://doi.org/10.1016/j.carbpol.2017.03.020.
[39] L. Tavares, E.E. Esparza Flores, R.C. Rodrigues, P.F. Hertz, C.P.Z. Noreña, Effect of deacetylation degree of chitosan on rheological properties and physical chemical characteristics of genipin-crosslinked chitosan beads, Food Hydrocoll. 106 (2020) 105876, https://doi.org/10.1016/j.foodhyd.2020.105876.
[40] M.M. Gaber, H. Shokry, A.H. Hassanin, S. Awad, M. Samy, M. Elkady, Novel palm peat lignocellulosic adsorbent derived from agricultural residues for efficient methylene blue dye removal from textile wastewater, Appl Water Sci 15 (2025) 32, https://doi.org/10.1007/s13201-025-02363-y.
[41] M.Y.K. Bryan, P.V. Chai, J.Y. Law, E. Mahmoudi, Graphene oxide-chitosan composite material as adsorbent in removing methylene blue dye from synthetic

wastewater, Mater. Today Proc. 64 (2022) 1587–1596, https://doi.org/10.1016/j.matpr.2022.03.092.
[42] S. Sowmya, G. Madhu, R. Sankannavar, S. Yerragolla, Adsorption using chitosan and nano zerovalent iron composite material for sustainable water treatment, Mater. Res. Express 8 (2021) 024001, https://doi.org/10.1088/2053-1591/abdb4d.
[43] M.-V. Nguyen, B.-K. Lee, Removal of dimethyl sulfide from aqueous solution using cost-effective modified chicken manure biochar produced from slow pyrolysis, Sustainability 7 (2015) 15057–15072, https://doi.org/10.3390/su71115057.
[44] M. Vakili, F. Gholami, H.M. Zwain, W. Wang, A. Mojiri, Z. Gholami, M. Tomas, A. S. Giwa, G. Cagnetta, Treatment of as(III)-contaminated food waste using alkali treatment and its potential application for methylene blue removal from aqueous solutions, J. Water Process Eng. 55 (2023) 104100, https://doi.org/10.1016/j.jwpe.2023.104100.
[45] V.S. Munagapati, V. Yarramuthi, Y. Kim, K.M. Lee, D.-S. Kim, Removal of anionic dyes (Reactive Black 5 and Congo Red) from aqueous solutions using Banana Peel Powder as an adsorbent, Environ. Saf. 148 (2018) 601–607, https://doi.org/10.1016/j.ecoenv.2017.10.075.
[46] S. Mallakpour, Z. Radfar, M. Feiz, Optimization of chitosan/tannic acid@ ZnFe layered double hydroxide bionanocomposite film for removal of reactive blue 4 using a response surface methodology, Int. J. Biol. Macromol. 209 (2022) 747–762, https://doi.org/10.1016/j.ijbiomac.2022.04.020.
[47] J. Geng, L. Lin, F. Gu, J. Chang, Adsorption of Cr(VI) and dyes by plant leaves: effect of extraction by ethanol, relationship with element contents and adsorption mechanism, Ind. Crop. Prod. 177 (2022) 114522, https://doi.org/10.1016/j.indcrop.2022.114522.
[48] H. Li, L. Miao, G. Zhao, W. Jia, Z. Zhu, Preparation of high-performance chitosan adsorbent by cross-linking for adsorption of Reactive Red 2 (RR2) dye wastewater, J. Environ. Chem. Eng. 10 (2022) 108872, https://doi.org/10.1016/j.jece.2022.108872.
[49] T. Karthikeyan, S. Rajgopal, L.R. Miranda, Chromium(VI) adsorption from aqueous solution by *Hevea brasilinesis* sawdust activated carbon, J. Hazard. Mater. 124 (2005) 192–199, https://doi.org/10.1016/j.jhazmat.2005.05.003.
[50] D. Sun, Z. Zhang, M. Wang, Y. Wu, Adsorption of reactive dyes on activated carbon developed from Enteromorpha prolifera, Am. J. Anal. Chem. 4 (2013) 17–26, https://doi.org/10.4236/ajac.2013.47A003.
[51] N. Tahari, P.L. de Hoyos-Martinez, N. Izaguirre, N. Houwaida, M. Abderrabba, S. Ayadi, J. Labidi, Preparation of chitosan/tannin and montmorillonite films as adsorbents for Methyl Orange dye removal, Int. J. Biol. Macromol. 210 (2022) 94–106, https://doi.org/10.1016/j.ijbiomac.2022.04.231.
[52] Z. Aksu, S. Ertuğrul, G. Dönmez, Single and binary chromium(VI) and Remazol Black B biosorption properties of Phormidium sp, J. Hazard. Mater. 168 (2009) 310–318, https://doi.org/10.1016/j.jhazmat.2009.02.027.
[53] X. Liu, R. Ma, X. Wang, Y. Ma, Y. Yang, L. Zhuang, S. Zhang, R. Jehan, J. Chen, X. Wang, Graphene oxide-based materials for efficient removal of heavy metal ions from aqueous solution: a review, Environ. Pollut. 252 (2019) 62–73, https://doi.org/10.1016/j.envpol.2019.05.050.
[54] C.G. Joseph, A. Wan Mohd, Q.K.S. Quek Kye Shane, K.S. Kogularama Sanmugam, Parametric and adsorption kinetic studies of Reactive Black 5 removal from textile simulated wastewater using oil palm (*Elais guineensis*) empty fruit bunch, J. Appl. Sci. 15 (2015), https://doi.org/10.3923/jas.2015.1103.1111.
[55] N.M. Thuan, N.T.M. Linh, N.T.T. Phuong, N.T.H. Duong, N.M. Hung, P.T. Tuyet, N. Van Dung, N.Q. Long, Ethanolamine-modified zeolite – chitosan beads as new adsorbents for carbon dioxide capture and crystal violet removal, Case Stud. Chem. Environ. Eng. 10 (2024) 100917, https://doi.org/10.1016/j.cscee.2024.100917.
[56] A. Samadi, L. Kong, W. Guo, M. Sillanpää, I. Boztepe, C. Song, Q. Zeng, S. Zhao, Standardized methodology for performance evaluation in using polyaniline-based adsorbents to remove aqueous contaminants, J. Environ. Chem. Eng. 12 (2024) 112650, https://doi.org/10.1016/j.jece.2024.112650.
[57] C. Ma, D. Liu, S. Deng, M. Vakili, Efficient chromium (VI) removal with zirconium oxide-carbon nanotubes via filtration-steam hydrolysis, Chem. Eng. Res. Des. 204 (2024) 664–672, https://doi.org/10.1016/j.cherd.2024.03.017.
[58] S. Hena, Removal of chromium hexavalent ion from aqueous solutions using biopolymer chitosan coated with poly 3-methyl thiophene polymer, J. Hazard. Mater. 181 (2010) 474–479, https://doi.org/10.1016/j.jhazmat.2010.05.037.
[59] N.N. Ramlee, R.M. Illias, S. Toemen, R.A. Rahman, R. Selvasembian, W. Fatriasari, N.I.W. Azelee, Adsorption study of isotherms, kinetics modelling, and thermodynamics of immobilized Candida rugosa lipase on metal oxide for esterification of waste cooking oil, Chem. Eng. Res. Des. 204 (2024) 249–268, https://doi.org/10.1016/j.cherd.2024.02.031.
[60] S. Pal, A.S. Patra, S. Ghorai, A.K. Sarkar, V. Mahato, S. Sarkar, R.P. Singh, Efficient and rapid adsorption characteristics of templating modified guar gum and silica nanocomposite toward removal of toxic reactive blue and Congo red dyes, Bioresour. Technol. 191 (2015) 291–299, https://doi.org/10.1016/j.biortech.2015.04.099.
[61] I.A. Lawal, D. Chetty, S.O. Akpotu, B. Moodley, Sorption of Congo red and reactive blue on biomass and activated carbon derived from biomass modified by ionic liquid, Environ. Nanotechnol. Monit. Manag. 8 (2017) 83–91, https://doi.org/10.1016/j.enmm.2017.05.003.
[62] J. Fito, M. Abewaa, T. Nkambule, Magnetite-impregnated biochar of parthenium hysterophorus for adsorption of Cr (VI) from tannery industrial wastewater, Appl Water Sci 13 (2023) 78, https://doi.org/10.1007/s13201-023-01880-y.
[63] R. Guo, W. Guo, H. Pei, B. Wang, X. Guo, N. Liu, Z. Mo, Polypyrrole deposited electrospun PAN/PEI nanofiber membrane designed for high efficient adsorption of chromium ions (VI) in aqueous solution, Colloids Surf. A Phys. Eng. Asp. 627 (2021) 127183, https://doi.org/10.1016/j.colsurfa.2021.127183.
[64] Y. Zhu, W. Dai, K. Deng, T. Pan, Z. Guan, Efficient removal of Cr (VI) from aqueous solution by Fe-Mn oxide-modified biochar, Water Air Soil Pollut. 231 (2020) 1–17, https://doi.org/10.1007/s11270-020-4432-2.
[65] D.-M. Liu, C. Dong, B. Xu, Preparation of magnetic kaolin embedded chitosan beads for efficient removal of hexavalent chromium from aqueous solution, J. Environ. Chem. Eng. 9 (2021) 105438, https://doi.org/10.1016/j.jece.2021.105438.
[66] M. Rastgordani, J. Zolgharnein, Simultaneous determination and optimization of titan yellow and reactive blue 4 dyes removal using chitosan@hydroxyapatite nanocomposites, J. Polym. Environ. 29 (2021) 1789–1807, https://doi.org/10.1007/s10924-020-01982-7.
[67] V. Singh, A.K. Sharma, D.N. Tripathi, R. Sanghi, Poly(methylmethacrylate) grafted chitosan: an efficient adsorbent for anionic azo dyes, J. Hazard. Mater. 161 (2009) 955–966, https://doi.org/10.1016/j.jhazmat.2008.04.096.
[68] L.H. Nguyen, H.P.N. Vu, P.V. Do, V.-P. Kha, N.T. Van, V.-T. Phan, D.-H. Huynh, T.-S. Le, Enhanced adsorption of Cr(VI) pollutants using CaFe2O4@rGO modified-biochar derived from mixture of black soldier flier exuviae and durian peel, J. Water Process Eng. 66 (2024) 106017, https://doi.org/10.1016/j.jwpe.2024.106017.
[69] T.M. Budnyak, M. Błachnio, A. Slabon, A. Jaworski, V.A. Tertykh, A. Deryło-Marczewska, A.W. Marczewski, Chitosan deposited onto fumed silica surface as sustainable hybrid biosorbent for Acid Orange 8 dye capture: effect of temperature in adsorption equilibrium and kinetics, J. Phys. Chem. C 124 (2020) 15312–15323, https://doi.org/10.1021/acs.jpcc.0c04205.
[70] R. de M. Ferreira, B.D. Ribeiro, D.M.A. Stapelfeldt, M. de F.R. Moreira, Treatment of water contaminated by ship oil: study of adsorption in a fixed-bed column, Analytica 5 (2024) 203–218, https://doi.org/10.3390/analytica5020013.
[71] A. Kara, E. Demirbel, N. Tekin, B. Osman, N. Beşirli, Magnetic vinylphenyl boronic acid microparticles for Cr(VI) adsorption: kinetic, isotherm and thermodynamic studies, J. Hazard. Mater. 286 (2015) 612–623, https://doi.org/10.1016/j.jhazmat.2014.12.011.
[72] A. Gupta, C. Balomajumder, Simultaneous adsorption of Cr(VI) and phenol onto tea waste biomass from binary mixture: multicomponent adsorption, thermodynamic and kinetic study, J. Environ. Chem. Eng. 3 (2015) 785–796, https://doi.org/10.1016/j.jece.2015.03.003.
[73] A.S. Abdulhameed, A. Hapiz, S.A. Musa, E. Kashi, R. Wu, Z.A. Alothman, A. H. Jawad, S. Algburi, Organically modified montmorillonite composited with magnetic glyoxal-chitosan Schiff base for reactive blue 19 dye removal: process optimization and adsorptive mechanism, Int. J. Biol. Macromol. 256 (2024) 128463, https://doi.org/10.1016/j.ijbiomac.2023.128463.
[74] A.H. Jawad, A.S. Abdulhameed, R. Selvasembian, Z.A. ALOthman, L.D. Wilson, Magnetic biohybrid chitosan-ethylene glycol diglycidyl ether/magnesium oxide/Fe3O4 nanocomposite for textile dye removal: Box–Behnken design optimization and mechanism study, J. Polym. Res. 29 (2022) 207, https://doi.org/10.1007/s10965-022-03067-6.
[75] P. Doondani, D. Panda, V. Gomase, K.R. Peta, R. Jugade, Novel chitosan-ZnO nanocomposites derived from Nymphaeaceae fronds for highly efficient removal of Reactive Blue 19, Reactive Orange 16, and Congo Red dyes, Environ. Res. 247 (2024) 118228, https://doi.org/10.1016/j.envres.2024.118228.
[76] R. El Kaim Billah, M.A. Islam, M.K. Nazal, L. Bahsis, A. Soufiane, Y. Abdellaoui, M. Achak, A novel glutaraldehyde cross-linked chitosan@acid-activated bentonite composite for effective Pb(II) and Cr(VI) adsorption: experimental and theoretical studies, Sep. Purif. Technol. 334 (2024) 126094, https://doi.org/10.1016/j.seppur.2023.126094.
[77] M. Vakili, S. Deng, L. Shen, D. Shan, D. Liu, G. Yu, Regeneration of chitosan-based adsorbents for eliminating dyes from aqueous solutions, Sep. Purif. Rev. 48 (2019) 1–13, https://doi.org/10.1080/15422119.2017.1406860.
[78] W. Wang, S. Zhou, R. Li, Y. Peng, C. Sun, M. Vakili, G. Yu, S. Deng, Preparation of magnetic powdered carbon/nano-Fe3O4 composite for efficient adsorption and degradation of trichloropropyl phosphate from water, J. Hazard. Mater. 416 (2021) 125765, https://doi.org/10.1016/j.jhazmat.2021.125765.